https://doi.org/10.5194/egusphere-2026-4950
Preprint. Discussion started: 28 September 2026

A framework to assess the impacts of urbanization on meteorological dynamics in megacities

Aasif Ahmad Wagay[1], Pauli Paasonen[2], Tuukka Petäjä[2], Victoria Sinclair[2†], Sarath Guttikunda[3,4], Shahzad Gani[1,2]*

[1]Centre for Atmospheric Sciences, Indian Institute of Technology Delhi, New Delhi, India
[2]Institute for Atmospheric and Earth System Research / Physics, University of Helsinki, Helsinki, Finland
[3]TRIP-Centre, Indian Institute of Technology Delhi, New Delhi, India
[4]Urban Emissions Information, Goa, India
[†] Deceased.

Correspondence to: Shahzad Gani (shahzadgani@iitd.ac.in)

Abstract. Urbanization modifies near-surface meteorology through changes in surface energy exchange, aerodynamic roughness, and boundary-layer development, with important implications for urban heat exposure and air quality. Although many studies have examined these effects in individual cities, a consistent, transferable framework for comparing urban meteorological signals across megacities remains lacking, and the extent to which such signals are shaped by the characteristics of the surrounding reference environment is rarely quantified. Here, we present a WRF based radial framework to diagnose urban rural contrast in near-surface meteorology and demonstrate its applicability across 20 global megacities during two contrasting months, May and October 2024. The framework characterizes radial variations in 2 m air temperature (T), 10 m wind speed (WS), and planetary boundary layer height (PBLH) using concentric 5 km circular rings extending 60 km from the city centres, from which a reproducible Urban–radial Contrast (URC) metric is derived. The framework further accounts for the influence of mixed land-ocean sampling and elevation differences within the reference environment, allowing the diagnosed URC to be decomposed into urbanization-attributed (URC_{UA}), ocean-attributed (URC_{OA}), and elevation-attributed components (URC_{EA}).

Application of the framework reveals consistent urban signatures in both months, characterized by warmer temperatures, deeper boundary layers, and weaker near-surface winds over urban cores relative to their surrounding reference environments, with stronger and more consistent contrasts in inland than in coastal megacities. Accounting for ocean and elevation-attributed contributions, however, substantially reshapes this picture in topographically complex cities. The strongest URC_{UA}-T occurs at night, reaching 6.1 and 6.0 °C in Delhi and Lahore, respectively, in October. Terrain complex cities such as Tehran and Mexico City exhibit the largest simulated nocturnal URC-T values of 7.6 and 5.1, respectively, which decrease to 3.6 and 3.2 (URC_{UA}-T) after accounting for the elevation-attributed contribution, although both remain among the strongest warming signals in the ensemble. Coastal cities exhibit much weaker nocturnal URC-T, generally ranging from 0.7 to 2.1 °C. The urban wind-speed deficit persists during both daytime and nighttime, with the strongest URC-WS occurring in Los Angeles (−2.0 m s^{-1}; nighttime, October) and Tehran (−1.8 m s^{-1}; daytime). In contrast, the strongest urban enhancement of PBLH occurs during

https://doi.org/10.5194/egusphere-2026-4950
Preprint. Discussion started: 28 September 2026

the daytime, with URC-PBLH reaching 592 m in Tehran (May), 489 m in Mexico City (May), and 526 m in Delhi (October). These diagnosed Urban–radial Contrasts, particularly their urbanization-attributed component, have important implications for pollutant dispersion and urban air quality in rapidly urbanising megacities.

Keywords: Megacities, Urban meteorology, Urbanization, Urban–radial contrast

1 Introduction

Rapid urbanization is reshaping local meteorology by replacing natural land cover with impervious and structurally complex urban surfaces that modify surface energy exchange, aerodynamic roughness, heat storage, and turbulent transport (Connors et al., 2013; Debbage and Shepherd, 2015). A prominent manifestation is the urban heat island (UHI), but the urban meteorological response extends beyond temperature alone to include changes in ventilation and mixing that are directly relevant to air quality (Li and Bou-Zeid, 2013; Wang et al., 2013; Yu et al., 2013). Prior studies have shown that urbanization can elevate nighttime temperatures (Yu et al., 2013), modify the diurnal evolution of planetary boundary layer height (PBLH) and associated $PM_{2.5}$ redistribution (Wang et al., 2021) and reduce near-surface wind speeds through increased roughness and altered surface properties (Qiao et al., 2023; Zhang et al., 2022a). Collectively, these changes can affect pollutant accumulation by suppressing dispersion and enhancing stagnation, while also influencing precipitation, humidity fields and PBLH that feed back on aerosol processes (Li et al., 2017; Petäjä et al., 2016; Rajeswari et al., 2021).

These effects are particularly important in megacities, where extensive land-surface modification, high anthropogenic activity, and large exposed populations frequently coincide (Marlier et al., 2016). As the number and size of megacities continue to grow worldwide, understanding how urbanization modifies local meteorology is becoming increasingly important. A megacity is generally defined as an urban agglomeration with a population exceeding 10 million, and the number of such cities is projected to increase from 33 in 2025 to approximately 47 by 2050, with most future growth occurring in Asia and Africa (United Nations, 2025). These regions are already experiencing severe environmental challenges, including deteriorating air quality, rapid land-use change, increasing energy demand, heightened climate vulnerability, and growing population exposure to environmental hazards (Babatola, 2018). As urban expansion continues, urbanization-driven changes in temperature, boundary-layer development, and ventilation are expected to become increasingly important controls on pollutant dispersion, population exposure, and the overall urban environment (Baklanov et al., 2016).

Beyond their societal importance, megacities span a wide range of climatic and geographic environments, making them well-suited for assessing how urbanization-driven meteorological changes vary across cities. However, despite substantial progress in both observational and modelling studies, robust inter-city comparison remains difficult. Much of the existing evidence is based on single-city or single-region analyses that use city-specific model configurations, analysis approaches, and rural reference definitions, thereby limiting direct comparability. In addition, broader environmental controls, particularly differences between coastal and inland settings, are rarely evaluated within a common analytical framework.

https://doi.org/10.5194/egusphere-2026-4950
Preprint. Discussion started: 28 September 2026

The geographic setting of a megacity fundamentally governs how urban land-surface forcing translates into meteorological modifications. In non-coastal (inland) environments, urban meteorological anomalies are primarily driven by localized changes in the surface energy balance, particularly enhanced sensible heat release and aerodynamic drag. Conversely, coastal megacities can exhibit urbanization effects that differ fundamentally from those of inland cities because the background meteorology is strongly shaped by land–sea thermal contrasts and associated sea–land breeze circulations. In such settings, mesoscale marine flows and their diurnal evolution can strongly influence near-surface temperature patterns, so that the apparent urban warming signal may reflect a superposition of urban forcing with sea-breeze cooling, land-breeze return flow, and, where present, slope or basin-related cold-air drainage. (Guan et al., 2016a; Liu et al., 2026). In dense coastal megacities, urban warming may interact with sea and land-breeze circulation to produce low-level convergence, stagnation, and modified ventilation, while land-surface heterogeneity and anthropogenic heat further affect local wind and moisture structure (Wang et al., 2017). Recent work also shows that urbanization itself can weaken sea–land breeze by changing wind direction and enhancing nighttime urban warming, while ocean warming reduces the daytime land–sea thermal contrast and further suppresses coastal ventilation (Xiao et al., 2023). More broadly, the coastal urban response is also sensitive to the larger meteorological regime, because strong synoptic or frontal forcing can modify or mask locally generated urban effects (Liu et al., 2026). Together, these factors make coastal cities physically distinct from inland cities and justify evaluating coastal and non-coastal urban responses separately within a common comparative framework.

In this study, we present a radial framework for diagnosing urban–rural meteorological contrasts from WRF simulations across 20 global megacities. The framework characterises 2 m air temperature (T), 10 m wind speed (WS), and planetary boundary layer height (PBLH) in concentric 5 km rings extending from the city centre to 60 km, resolves local daytime and nighttime radial structure, and summarises inner–outer contrasts using the Urban–radial contrast (URC) metric. In addition to characterizing mean radial behaviour, the framework retains ring-wise distributions to quantify within-ring spatial heterogeneity and explicitly accounts for the influence of mixed land–ocean sampling and elevation differences within the reference environment, thereby decomposing the derived URC into urbanization-attributed (URC_{UA}), ocean-attributed (URC_{OA}), and elevation-attributed (URC_{EA}) components. The central objective is therefore not only to determine how urbanization modifies near-surface meteorology, but also to establish whether these modifications can be quantified consistently across diverse cities and contrasting time periods using a common analytical framework. Demonstrating such robustness requires evaluation in both spatial and temporal dimensions, i.e. across a wide range of cities and across contrasting seasonal meteorological conditions. This is especially relevant for megacities, where the extensive urban built-up areas and the associated strong urban forcing often make urban-induced meteorological changes more distinguishable from background variability, and thus more suitable for intercomparison within a common framework. This paper focuses on the framework and its meteorological interpretation. Future work will extend this framework towards urban air-quality sensitivity, reduced-complexity modelling, and longer-term climatological applications.

https://doi.org/10.5194/egusphere-2026-4950
Preprint. Discussion started: 28 September 2026

2 Methodology

2.1 WRF domain setup and simulation design

We performed two separate month-long simulations for May 2024 and October 2024 for each megacity using WRF-ARW version 4.3. The model configuration employed three two-way nested domains (centred at the city) with horizontal grid spacings of 36 km, 12 km, and 4 km, and all framework analyses were conducted for the innermost domain (d03). Initial and lateral boundary conditions were provided by National Centers for Environmental Prediction (NCEP) Final (FNL) operational global analysis data, available every 6 h at 1° × 1° spatial resolution. May and October 2024 were selected to represent contrasting meteorological conditions across the cities, thereby allowing the framework to be evaluated under different background meteorological regimes while maintaining computational feasibility. The simulations used 41 vertical levels, with the model top set at 50 hPa, and hourly model output was archived for analysis. To capture fine-scale surface–atmosphere interactions, these levels were clustered near the ground, yielding the lowest model layer thickness of approximately 15 m, with 21 levels strategically distributed within the lowest 3000 m of the atmosphere. We excluded the first 24 h of each simulation to account for model spin-up. The physics configuration included WSM6 microphysics, RRTMG longwave and shortwave radiation, the revised MM5 surface-layer scheme, the Noah land-surface model, and the YSU planetary boundary-layer scheme. Convection was parameterized only in the outermost domain using the Kain-Fritsch scheme, whereas cumulus parameterization was switched off in the 12 and 4 km inner domains. We did not use an explicit urban canopy model in these simulations. Urban effects were therefore represented through the default bulk urban land-use treatment in WRF. Accordingly, the simulations were designed to capture urbanization-related mesoscale meteorological responses (Lo et al., 2007) , rather than detailed street-canyon-scale processes. A complete summary of the WRF configuration is provided in the Supplement (Table S1).

2.2 City selection and coastal vs non-coastal categorisation

We selected 20 global megacities to evaluate the proposed framework across a broad range of climatic, geographic, and urban settings. For each city, a representative city-centre coordinate was defined and used as the reference point for all distance-based calculations. Hourly WRF outputs were converted from UTC to local time using a fixed city-specific UTC offset so that daytime, nighttime, and mean (full month) analyses were evaluated consistently in local time. To further examine the influence of geographic setting on framework performance, the selected cities were grouped into coastal and non-coastal categories. This classification was used to assess whether marine influence alters the radial structure and magnitude of URC in T, PBLH, and WS, and whether the framework captures these differences consistently across contrasting environments. The city list, classification, and associated metadata are summarized in the **Error! Reference source not found.**.

Table 1: Selected megacities, their city-centre coordinates, UTC offsets used for local-time conversion, and coastal/non-coastal classification. The population and LULC data are taken from the United Nations World Urbanization Prospect 2025

https://doi.org/10.5194/egusphere-2026-4950
Preprint. Discussion started: 28 September 2026

No	City	Lat	Lon	UTC offset	Category	Pop (M)	Land Area (km²)	Built-up Area (km²)
1	Delhi	28.61	77.21	+5.5	Non-coastal	30.22	2101	563
2	Beijing	39.90	116.40	+8.0	Non-coastal	17.01	1713	487
3	Paris	48.85	2.35	+2.0	Non-coastal	9.38	1381	372
4	Cairo	30.04	31.24	+2.0	Non-coastal	25.56	1645	385
5	Mexico City	19.43	-99.13	-6.0	Non-coastal	17.73	2097	643
6	Moscow	55.76	37.62	+3.0	Non-coastal	14.52	1561	325
7	Dhaka	23.81	90.41	+6.0	Non-coastal	36.58	6812	456
8	Tehran	35.68	51.38	+3.5	Non-coastal	9.17	786	250
9	Johannesburg	-26.20	28.04	+2.0	Non-coastal	7.07	1445	406
10	São Paulo	-23.55	-46.63	-3.0	Non-coastal	18.95	2044	678
11	London	51.50	-0.12	+1.0	Non-coastal	10.41	1646	426
12	Lahore	31.54	74.34	+5.0	Non-coastal	15.15	967	265
13	New York	40.71	-74.00	-4.0	Coastal	13.92	2691	679
14	Barcelona*	41.38	2.17	+2.0	Coastal	5.73	-	-
15	Tokyo	35.68	139.76	+9.0	Coastal	33.41	5148	1521

https://doi.org/10.5194/egusphere-2026-4950
Preprint. Discussion started: 28 September 2026

16	Shanghai	31.23	121.47	+8.0	Coastal	29.55	3130	803
17	Lagos	6.45	3.39	+1.0	Coastal	12.79	1231	453
18	Los Angeles	34.05	-118.25	-7.0	Coastal	12.74	3699	1239
19	Mumbai	19.08	72.88	+5.5	Coastal	20.20	740	152
20	Istanbul	41.00	28.97	+3.0	Coastal	15.015	1268	304
**Not technically a megacity yet, but included to improve the balance of Global North and South megacities*								

2.3 Radial-ring framework methodology

We applied a concentric radial-ring analysis to quantify the spatial structure of urban influence around each megacity. All analyses were performed on the innermost WRF domain (d03). Great-circle distances between the prescribed city-centre coordinate and every WRF grid cell were calculated using the haversine formula, producing a two-dimensional distance field, $D(x, y)$, expressed in kilometres. This distance field was then used to assign each native WRF grid cell to one of 12 concentric annular bins spanning 0–60 km from the city centre, at 5 km intervals. All statistics were calculated directly on the native model grid by aggregating grid cells belonging to the same radial bin. Each ring was represented by its midpoint distance (2.5, 7.5, ..., 57.5 km).

A common radial extent of 60 km was selected to provide sufficient spatial coverage to capture the transition from the urban core to the surrounding background/rural environment while maintaining a consistent analysis framework across all megacities. Applying the same radial extent to all cities facilitates direct inter-city comparison of urbanization-induced meteorological gradients and urban–rural contrast. However, because urban spatial extents differ substantially among megacities, the outer rings of some highly extended metropolitan regions may still contain considerable urban land fractions and therefore may not represent a strictly true rural reference environment. This limitation should be considered when interpreting radial gradients and inner–outer contrasts.

For each meteorological variable analyzed (T, PBLH, and WS), model timestamps were first converted from UTC to local standard time using a fixed city-specific UTC offset. Here, T was converted from K to °C, and WS was calculated from the 10 m zonal and meridional wind components as

$$WS_{10} = \sqrt{U_{10}^2 + V_{10}^2} \quad (1)$$

Daytime and nighttime periods were then defined using local astronomical sunrise and sunset times computed at the city-centre coordinate using the Astral library in Python. For each local date, an hourly timestep was classified as daytime when the local time satisfied $t_{\text{local}} \in [t_{\text{sunrise}}, t_{\text{sunset}})$, and as nighttime otherwise. Daytime and nighttime hours were aggregated separately to produce mean daytime and nighttime two-dimensional fields (i.e. gridded horizontal fields of T, PBLH, and WS over the analysis domain). Although a full period mean field was also computed during processing, the analyses presented here focus

https://doi.org/10.5194/egusphere-2026-4950
Preprint. Discussion started: 28 September 2026

on the daytime and nighttime composites. For each radial ring, we calculated spatial distribution statistics including the mean, median, 10th percentile (p10), 25th percentile (p25), 75th percentile (p75), and 90th percentile (p90). These statistics were used to characterise both the central tendency and the within-ring spatial heterogeneity of the urban meteorological signal. In the analyses presented here, mean ring values were used to calculate URC.

2.4 Urban–radial contrast (URC)

In addition to continuous radial profiles, we derived a compact scalar metric, termed URC, to summarize the strength of the urban signal for each city. URC compares an inner urban-core zone (0–15 km) with an outer background zone (45–60 km) using the radial-ring mean values. For each city, variable, and period, we calculated the inner-zone average, X_{in}, and the outer-zone average, X_{out}, from the mean values of rings within the respective distance ranges. URC was then defined as

$$URC = X_{\text{in}} - X_{\text{out}} \tag{2}$$

A positive URC indicates higher values in the urban core than in the outer/rural reference zone, whereas a negative URC indicates lower core values relative to the reference background. The URC was calculated separately for T, PBLH, and WS, and for the daytime and nighttime periods. This metric provides a compact basis for comparing urban–rural meteorological contrasts across cities, seasons, and coastal versus non-coastal settings.

2.5 Land-use and elevation data

We characterized the land-use/land-cover (LULC) composition and topographic variability within the 60 km radial analysis window for each city. LULC and elevation fields were extracted directly from the WRF output, where the static geographical datasets had already been interpolated to the d03 model grid resolution during preprocessing. Although the WRF land-use field is based on the MODIS 20-category dataset, the present analysis used the interpolated model-grid fields rather than the native source-resolution data. For interpretation, the land-use categories were aggregated into six broad classes: urban, cropland, forest, other vegetation (grass/shrub), barren, and water. The model-grid elevation field was used to characterise topographic variability within the same analysis domain. For consistency across all cities, the same 0–60 km radial window was used for the LULC and elevation analyses.

2.6 Evaluation of WRF simulations against ERA5

To assess whether the WRF simulations reproduced the large-scale meteorological state with sufficient realism, the simulated near-surface meteorological fields (T, PBLH, and WS) were evaluated against ERA5 reanalysis for May and October 2024. Model performance was assessed using both hourly data and daytime and nightime composite averages to maintain consistency with the analysis framework adopted in this study. Standard statistical metrics, including the Pearson correlation coefficient (r), root mean square error (RMSE), and mean bias, were used to evaluate model performance. The complete evaluation, including methodology, statistical metrics, and comparison figures, is presented in the Supplement (Sect. S1; Figs. S1–S2).

https://doi.org/10.5194/egusphere-2026-4950
Preprint. Discussion started: 28 September 2026

Overall, the evaluation indicates that the WRF simulations reproduce the principal temporal and inter-city variability of the analysed meteorological variables, providing confidence for the subsequent relative urban-effect analysis.

2.7 Quantifying elevation and ocean attributions to derived Urban–radial Contrast

Although the proposed radial framework is designed to quantify urban meteorological responses, the sampled outer environment may also contain background environmental gradients unrelated to urbanization. In particular, radial temperature contrasts can be influenced by systematic elevation differences between the urban core and the surrounding terrain (elevation), while coastal cities may exhibit mixed land–ocean sampling within the outer reference rings. To improve the physical interpretation of the isolated urban signals and enhance inter-city comparability, two complementary methodological adjustments were incorporated into the framework.

First, to minimize the influence of elevation-induced temperature differences on near-surface air temperature, T was adjusted to a common reference elevation prior to radial aggregation. For each city, the reference elevation (Z_{ref}) was defined as the mean terrain height (HGT) of all grid cells within the 0–5 km urban core. Temperature at each grid cell within the analysis domain was then adjusted to this common reference elevation using a constant environmental lapse rate of 6.5 K km^{-1},

$$T_{\mathrm{adj}} = T_{\mathrm{sim}} + \Gamma(Z_{\mathrm{sim}} - Z_{\mathrm{ref}}) \quad (3)$$

where T_{adj} is the elevation-adjusted temperature, T_{sim} is the original WRF-simulated near-surface temperature, Γ is the environmental lapse rate, and HGT is the terrain elevation of each grid cell. The elevation-adjusted temperature field was subsequently aggregated into the same 5 km concentric rings used in the standard analysis, and both the radial temperature distributions and the corresponding URC were recomputed using the adjusted temperatures. This elevation adjustment was applied exclusively to temperature fields because the environmental lapse rate provides a physically based first-order approximation for elevation-induced temperature differences. No analogous adjustment was applied to PBLH or WS, whose responses to terrain are governed primarily by more complex dynamical processes rather than by a simple dependence on elevation.

Second, to account for the influence of coastal reference environments, the radial analysis for coastal cities was repeated using a land-only mask that excluded ocean grid cells from all radial statistics. This procedure was applied consistently to the radial distributions and, consequently, to the corresponding URC calculations for T, PBLH, and WS, thereby providing a land-based reference environment for coastal cities while leaving the simulated meteorological fields unchanged.

For clarity and consistency throughout the manuscript, four analysis states are distinguished. Simulated refers to the original WRF output without any environmental adjustment. Ocean-adjusted refers to analyses in which ocean grid cells are excluded while retaining the original simulated meteorological fields. Elevation-adjusted refers to analyses in which only the elevation adjustment is applied. Combined-adjusted refers to analyses in which both the ocean adjustment and the elevation adjustment

https://doi.org/10.5194/egusphere-2026-4950
Preprint. Discussion started: 28 September 2026

are applied. Correspondingly, the computed URCs from each analysis state are denoted as $URC_{simulated}$, $URC_{ocean\text{-}adjusted}$, $URC_{elevation\text{-}adjusted}$, and $URC_{combined\text{-}adjusted}$, respectively. These terms are used consistently throughout the manuscript when discussing both the radial profiles and the corresponding URC metrics.

The four analysis states also enable decomposition of the derived URC into contributions associated with ocean sampling and elevation differences within the reference environment. Accordingly, the derived URC can be expressed as

$$URC_{\text{simulated}} = URC_{\text{UA}} + URC_{\text{OA}} + URC_{\text{EA}} \tag{4}$$

$$URC_{\text{OA}} = URC_{\text{simulated}} - URC_{\text{ocean\_adjusted}} \tag{5}$$

$$URC_{\text{EA}} = URC_{\text{ocean\_adjusted}} - URC_{\text{combined\_adjusted}} \tag{6}$$

$$URC_{\text{UA}} = URC_{\text{combined\_adjusted}} \tag{7}$$

For simplicity, the $URC_{simulated}$ is hereafter referred to simply as URC. URC_{OA} represents the component of the derived URC attributed to mixed land–ocean sampling within the reference rings, while URC_{EA} represents the component attributed to elevation differences between the urban core and the surrounding reference environment. The remaining component, URC_{UA}, represents the urbanization-attributed URC after accounting for both quantified environmental influences and is equivalent to the $URC_{combined\text{-}adjusted}$. This decomposition provides a more physically consistent basis for interpreting characterized urban–rural meteorological contrasts and for inter-city comparison.

3. Land-use and topographic characteristics of megacities

As the proposed framework quantifies both the radial evolution of urban meteorological signals and the associated inner–outer contrasts, the interpretation of the derived patterns depends not only on urban form but also on how the surrounding reference environment is defined and sampled (Hurduc et al., 2024; Kumar et al., 2017; Martin-Vide et al., 2015; Peng et al., 2024). We therefore first examine the LULC composition and topographic variability within the 0–60 km radial domain to provide physical context for the simulated meteorological gradients across the 20 megacities (Fig. 1). As described in Sect. 2.5, LULC was grouped into six classes: urban (built-up), cropland, forest, other vegetation (grass/shrub), barren, and water. Figure 1 summarizes ring-wise LULC fractions and elevation statistics for 5 km wide ring bands in non-coastal (n = 12) and coastal (n = 8) cities. Azimuthal LULC distributions around each city centre are also shown in the subplots.

Most non-coastal cities exhibit a clear radial urban-to-non-urban land-cover transition i.e. a classical urban–rural transition, with strongly urban-dominated inner rings (typically ≳90 % urban within 0–15 km; e.g., Delhi and Beijing) and markedly reduced urban fractions beyond ~30 km (typically <20 %), where surrounding landscapes are dominated by cropland in several cities (e.g., cities in Asia and Europe, Fig. 1). Delhi is overwhelmingly built-up in the 0–10 km core and transitions rapidly to cropland, which becomes dominant by ~25–30 km; terrain variability is minimal (p10–p90 elevation range <100 m within 60 km). Beijing exhibits a spatially uneven built-up structure embedded within a cropland-dominated surround, along with an

https://doi.org/10.5194/egusphere-2026-4950
Preprint. Discussion started: 28 September 2026

outward increase in elevation (mean ≈50 m in the core rising to ≈200 m by ~45–50 km; p90 >600 m), consistent with foothill influence (Wu et al., 2015).

Paris and London also retain strongly urban inner rings, despite more fragmented surrounding development, and transition to largely cropland-dominated outer zones beyond ~25-30 km. Moscow differs from these cities in having a forest-dominated outer reference environment beyond ~20–25 km and low-relief terrain. Mexico City stands out because the reduction in urban fraction with distance occurs within a strongly elevated basin setting, where elevation heterogeneity increases markedly away from the city centre (p90 rising from ~2.25 km in the core to >3.2 km in the 25–45 km rings), consistent with basin confinement and the strong role of topography reported for Mexico City's UHI climatology (Jauregui, 1997). These differences are important because cropland, forest, and terrain-dominated outer rings do not constitute equivalent background conditions.

Across inland cities, these outer-ring environments can be grouped into distinct physical regimes. Several megacities are embedded primarily in cropland surroundings (e.g., Delhi, Lahore, Paris, London and Dhaka; Fig. 1), implying that seasonal and management-driven variability in rural evapotranspiration, including irrigation, can modulate the daytime urban-rural thermal contrast (Kumar et al., 2017). In contrast, cities with forest-dominated outer rings (e.g. Moscow and São Paulo) are more likely to maintain stronger daytime evaporative cooling in the surrounding environment, which can enhance urban–background contrasts under comparable synoptic forcing (Arnfield, 2003).

In coastal cities, the outer rings frequently include substantial water fractions (e.g. Istanbul, Barcelona, Lagos, Mumbai, and Shanghai; Fig. 1), indicating that radial sampling often captures mixed land–sea environments rather than a purely terrestrial rural reference. This is meteorologically important because land–sea thermal contrasts can drive sea-breeze circulations that advect cooler marine air inland and interact with urban heat-island circulations, thereby reshaping near-surface temperature gradients and their spatial structure (Bauer, 2020; Hu et al., 2022). The LULC maps also show that Tokyo retains high urban fractions even at the largest radii; consequently, the outer ring cannot be interpreted as a strictly rural reference, and the resulting urban–outer contrasts should therefore be regarded as conservative estimates for Tokyo.

Topography also varies markedly among cities, particularly among the non-coastal group. Several cities exhibit strong relief within the 60 km analysis window (e.g. Tehran, Los Angeles, Mexico City, São Paulo, and Johannesburg), whereas others are comparatively flat. Because near-surface temperature structure and boundary-layer evolution are sensitive to elevation, slope, and terrain-driven circulations. Therefore, the high-relief rings can introduce non-urban gradients that are independent of land-use change. Observational evidence further suggests that urban–rural thermal contrasts can vary with elevation in some settings, reinforcing the need to interpret radial gradients in high-relief cities as a combination of urban effects and orographic background structure (Tang et al., 2022). Collectively, these LULC and elevation characteristics highlight a key advantage of the proposed framework: it not only resolves the radial structure of urban meteorological signals but also provides the physical context needed to distinguish gradients primarily associated with urbanization from those additionally shaped by coastline influence, topography, and reference-environment heterogeneity.

https://doi.org/10.5194/egusphere-2026-4950
Preprint. Discussion started: 28 September 2026

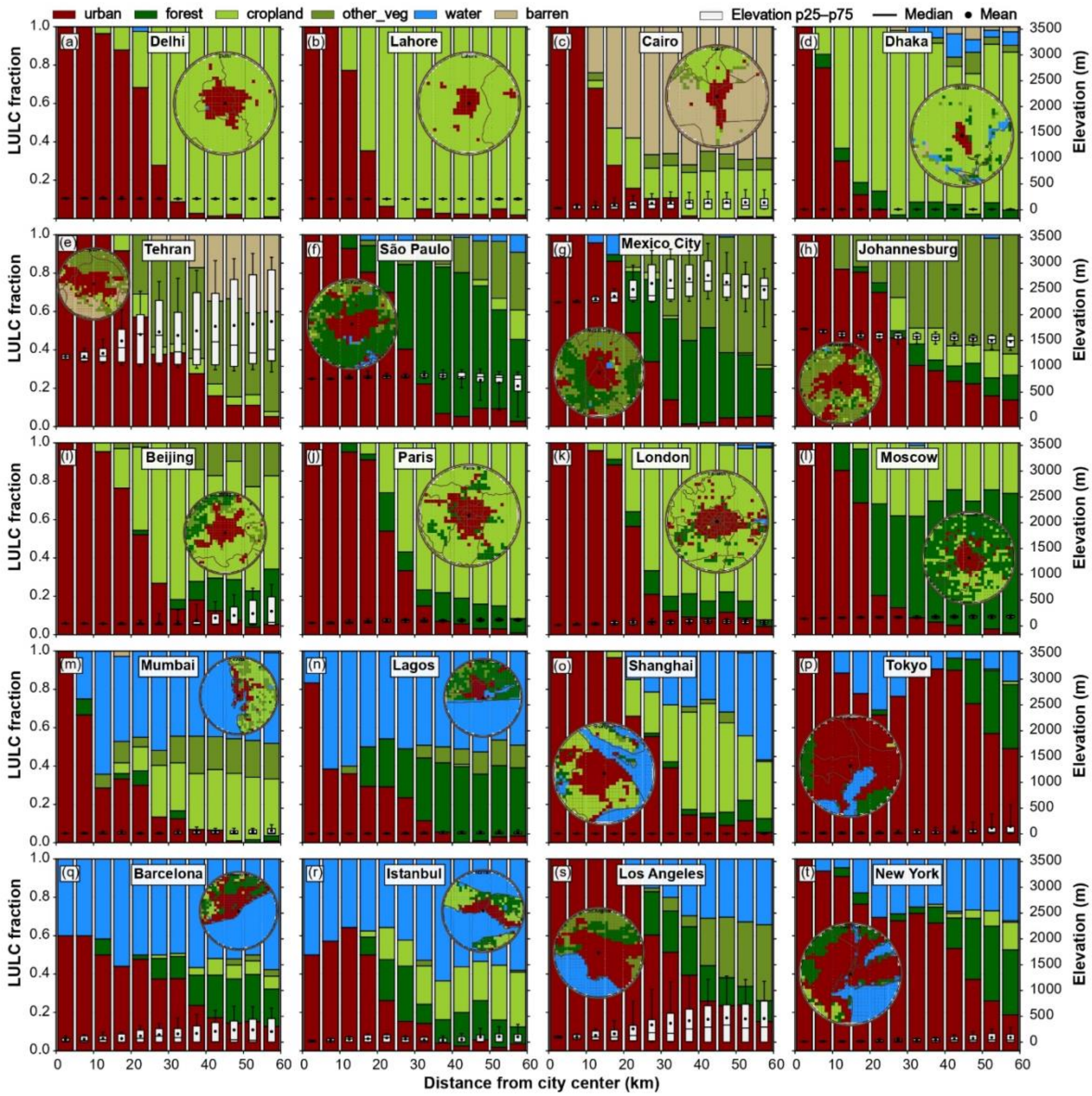

Figure 1: LULC fractions and elevation distribution across 20 megacities. Each panel displays ring-wise LULC fractions in 5 km bands, extending from the city centre to 60 km, with stacked bars representing the fractional contributions of urban, forest, cropland, other vegetation, water, and barren classes. Circular inset maps provide the corresponding spatial LULC (within a 60 km radius) for each city. Elevation variability for each ring is overlaid using box-and-whisker symbols, where the box denotes the interquartile range (p25–p75), whiskers denote p10–p90, the horizontal line marks the median, and the dot indicates the mean. Panels are arranged consistently, with non-coastal cities shown in the upper three rows and coastal cities in the lower two rows.

https://doi.org/10.5194/egusphere-2026-4950
Preprint. Discussion started: 28 September 2026

4 Radial change in meteorology across megacities

4.1 Radial change in near-surface temperature

Error! Reference source not found. presents simulated ring-wise distributions of temperature as a function of radial distance from each city centre (0–60 km) for October 2024, shown separately for daytime and nighttime conditions and grouped into non-coastal and coastal cities. The corresponding May results are provided in the Supplement (Fig. S4). The interquartile range (IQR) and p10–p90 whiskers quantify the spatial variability among grid cells within each annulus, reflecting heterogeneity associated with mixed land-cover composition, terrain, and surface characteristics sampled by each ring rather than temporal variability. Across the 20-city ensemble, the simulated temperature profiles generally decrease from the urban core towards the outer rings in both months, although the magnitude and smoothness of this decline vary considerably depending on the surrounding land-cover regime, coastal influence, terrain complexity, and prevailing meteorological conditions (Park et al., 2024; Stewart and Oke, 2012).

Among the non-coastal (inland) megacities, cities embedded within extensive cropland landscapes, including Delhi, Lahore, Dhaka, and Beijing, exhibit some of the clearest urban-centred warming structures in both months, particularly during nighttime. As illustrated by the land-use and elevation maps (Fig. 1), these cities exhibit only minor elevation variations across the 60 km analysis domain, indicating that the observed temperature patterns are primarily controlled by land-surface characteristics rather than terrain effects. This behaviour is especially evident in Delhi and Lahore, where the nocturnal inward warming is considerably stronger in October than in May, consistent with pronounced urban–agricultural thermal contrasts and the Delhi-region urban heat island characteristics previously documented using Local Climate Zone (LCZ) frameworks (Budhiraja et al., 2019, 2020). European cities with similarly cropland-dominated surroundings, such as Paris and London, also exhibit well-defined urban warming, although with weaker gradients than the South Asian megacities and with magnitudes that vary more strongly with prevailing meteorological conditions.

These cropland-dominated cities also display relatively pronounced daytime urban-core warming. A plausible explanation is enhanced evaporative cooling over surrounding vegetated landscapes, which suppresses rural daytime temperatures through increased latent heat fluxes (Li et al., 2019). In South Asian cities, this contrast becomes more pronounced in October, possibly reflecting residual post-monsoon soil moisture that helps maintain cooler agricultural surfaces relative to the urban core. However, during May, stronger solar heating and the development of a deeper convective boundary layer promote more efficient turbulent mixing, thereby reducing urban–rural thermal contrasts and producing flatter daytime temperature distributions, particularly over Delhi and Lahore (Cui and De Foy, 2012; Zhang et al., 2022b).

The spatial variability within each ring, represented by the IQR and p10–p90 whiskers, generally increases towards the outer rings, where the sampled environment becomes increasingly heterogeneous, incorporating mixed vegetation, fragmented urban development, water bodies, and complex terrain rather than a relatively homogeneous rural landscape. This behaviour is particularly evident in terrain-complex inland cities such as Tehran, São Paulo, Mexico City, and Johannesburg, where simulated radial temperature structures are less monotonic than those observed in flatter inland cities. Tehran and Mexico City,

https://doi.org/10.5194/egusphere-2026-4950
Preprint. Discussion started: 28 September 2026

for example, exhibit pronounced urban-core warming together with substantial variability in the outer rings, indicating that the observed temperature patterns reflect the combined influence of urbanization and background elevation gradients. Johannesburg presents an even more distinctive case, with a weak or locally reversed daytime radial temperature profile, illustrating how environmental controls can partially offset the urban thermal signal. These observations are consistent with previous studies highlighting the influence of topography, vegetation, and basin-scale circulation on urban thermal climatology (Jahangir and Moghim, 2019; Park et al., 2024; Zargari et al., 2025). An important strength of the proposed framework is that it explicitly captures this spatial heterogeneity, thereby identifying cities where the diagnosed urban–rural thermal contrast is influenced not only by urbanization but also by variability in the surrounding terrain and land-cover composition.

The elevation-adjusted analysis (Sect. 2.7; Figs. S1 and S2) further strengthens the interpretation of these temperature distributions. In low-relief cities, including Delhi, Lahore, Dhaka, Paris, London, and Cairo, elevation adjustment produces only negligible changes, confirming that the observed radial temperature profiles are primarily associated with urbanization rather than systematic elevation differences between the urban core and surrounding rings. By contrast, substantial changes occur in terrain-complex cities such as Tehran, Mexico City, São Paulo and Johannesburg. Following elevation adjustment, the outward cooling tendency is reduced, within-ring variability decreases, and the radial temperature structures become more coherent, closely resembling the canonical urban heat island structure. Johannesburg provides a particularly illustrative example. In the originally simulated daytime distribution, the city exhibits an apparent decrease in temperature towards the urban core; however, after elevation adjustment, this changes to the expected UHI pattern, demonstrating that the initial negative contrast was largely attributable to the higher elevation of the urban core compared to the surrounding reference environment. Similarly, pronounced improvements are also evident in coastal terrain-complex cities such as Los Angeles and Barcelona, where the radial temperature distributions become flatter after elevation adjustment, indicating that part of the apparent outward cooling in the simulated analysis was attributable to elevation differences in the surrounding terrain.

Relative to the non-coastal group, coastal megacities generally exhibit a weaker, smoother radial decay in temperature profiles, although most still retain a clearer urban warming signal at night than during the day. This nocturnal enhancement is consistent with canonical canopy-layer UHI behaviour, but in coastal settings, the temperature structure is often damped or redistributed by marine influence. In particular, land–sea thermal contrasts and sea/land-breeze ventilation can advect cooler maritime air inland, enhance mixing, and shift the warm anomaly depending on coastline geometry and background flow (Bauer, 2020; Guan et al., 2016b) as illustrated by the corresponding spatial temperature fields (Figs. S14–S17). In addition, when the outer rings include ocean grid cells, the relatively warm nighttime marine surface, owing to its high heat capacity, can further dampen the diagnosed urban–rural thermal contrast (Xiao et al., 2023). These combined effects help explain the smoother coastal behaviour, especially evident in cities such as Istanbul, Lagos, and Shanghai. Compared with inland cities, coastal megacities also exhibit substantially greater within-ring variability, particularly beyond approximately 30 km from the urban core, as reflected by the broader IQRs and p10–p90 whiskers. Cities like Los Angeles and New York retain more distinct nocturnal radial structure (prior to any adjustment). Tokyo also shows persistent inward warming, but this should be interpreted conservatively because the outer rings remain substantially urbanized in the Tokyo megaregion, reducing the effective urban–

https://doi.org/10.5194/egusphere-2026-4950
Preprint. Discussion started: 28 September 2026

background contrast. Los Angeles is particularly noteworthy because its coastal-basin setting allows land–sea breeze circulations to interact with terrain-driven flows, while the outer rings also sample higher-elevation sectors; together, these factors increase spatial heterogeneity and help maintain a more distinct radial temperature structure than in several other coastal cities. These coastal and elevation effects will be further discussed in more detail in Section 5

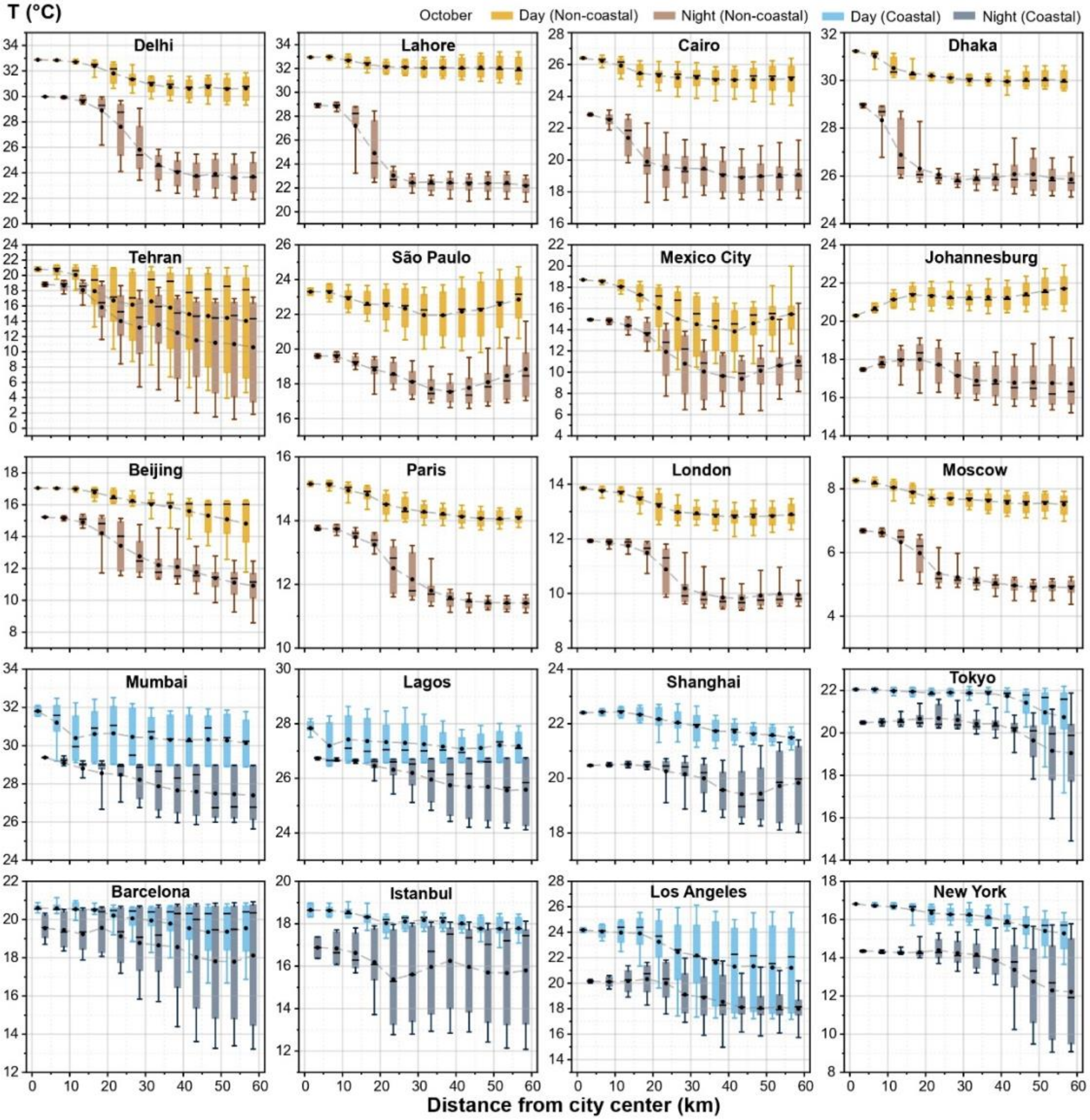

Figure 2: Radial distributions of simulated temperature (T) across the 20 megacities for October. Each city panel shows T statistics in 5 km radial bands from the city centre to 60 km, with non-coastal cities arranged in the upper three rows and coastal cities in the lower two rows. Within each group, cities are arranged to broadly group similar temperature ranges, with topographically complex cities intentionally placed in the same row. Daytime and nighttime distributions are shown separately, with colours distinguishing day and night for the two city groups. Boxes represent the interquartile range (p25–p75), whiskers represent p10–p90, and black

https://doi.org/10.5194/egusphere-2026-4950
Preprint. Discussion started: 28 September 2026

markers connected by dashed lines indicate the ring-wise mean. Note that the y-axis temperature ranges vary across individual city panels to accommodate distinct local thermal amplitudes. The visual density of the horizontal gridlines directly reflects the magnitude of the temperature range in each city. The identical city order and panel arrangement in both months allow direct comparison of the radial thermal structure under contrasting seasonal conditions.

4.2 Radial Change in PBLH

Figure 3 presents the ring-wise distributions of simulated PBLH as a function of radial distance from the city centre (0–60 km) for October 2024, resolved separately for daytime and nighttime composites and for non-coastal and coastal city groups. The corresponding May distributions are provided in the Supplement (Fig. S7). Across the 20-city ensemble, PBLH exhibits the expected diurnal cycle, with substantially deeper daytime mixed layers and shallower nighttime layers (Liu and Liang, 2010). A recurring feature, particularly in non-coastal cities, is deeper PBLH in the inner rings and a tendency for PBLH to decrease towards the outer rings, indicating enhanced boundary layer height over the urban core. This behaviour is consistent with stronger sensible heating and mechanically generated turbulence over urban surfaces, both of which promote boundary-layer development relative to the surrounding background (Barlow, 2014). The within-ring spread is also generally larger during the daytime than at night, reflecting stronger spatial variability under convective conditions when turbulence and mixing are more vigorous than in the nocturnal stable boundary layer.

Within the non-coastal group, the radial structure of PBLH differs systematically across cities and between seasons. Cities with relatively low-relief agrarian surroundings, such as Delhi, Lahore, Dhaka, Paris, and London, generally show strong day–night separation and a comparatively clear radial decay with distance, indicating that the framework captures the urban enhancement of boundary-layer height against a relatively uniform land-based background. Seasonal differences are especially evident during the daytime. In several Northern Hemisphere cities, May exhibits markedly deeper daytime PBLH than October, but often with flatter radial gradients because stronger convective mixing reduces the relative separation between the inner and outer rings. This is particularly evident in Delhi and Lahore, where daytime PBLH in May is very deep throughout the domain, and the radial gradient is comparatively weak. In contrast, October clearly expresses urban-core enhancement of daytime PBLH in several inland cities, including Delhi, Lahore and Mexico City, where the inner rings retain substantially deeper mixed layers than the surrounding outer rings. At night, inland cities generally show much shallower PBLH than during the day, with a clearer but smaller urban enhancement, reflecting the stronger influence of local stability. In the Southern Hemisphere, the two months correspond to different seasons; accordingly, cities such as Johannesburg and São Paulo show May profiles that are more consistent with cooler-season boundary-layer behaviour than October.

Terrain-complex inland cities further highlight the value of the framework. Mexico City and Tehran exhibit pronounced radial structure and broad within-ring distributions, especially at larger radii, again suggesting that the observed PBLH gradients reflect a combination of urban forcing and elevation-driven heterogeneity rather than urbanization alone. In Mexico City, the daytime radial decline is strong in both months but particularly clear in October, while the broad outer-ring spread is consistent with its elevated basin setting. Tehran likewise shows a strong daytime radial gradient, but with substantial spread at larger radii, again indicating that terrain complexity contributes to the derived structure.

https://doi.org/10.5194/egusphere-2026-4950
Preprint. Discussion started: 28 September 2026

In the coastal cities, the mean daytime radial structure of PBLH is generally smoother and often weaker than in the inland group, while the within-ring distributions are frequently broader, particularly in the middle and outer rings. This behaviour reflects land–sea breeze influences, which introduce spatially varying stability and thereby modify inland mixed-layer development depending on the background flow (Melecio-Vázquez et al., 2018). Nevertheless, some coastal cities, including Tokyo, Shanghai, and New York, still show indications of enhanced PBLH near the urban core, although the magnitude of the radial decay is usually weaker than in the non-coastal group. The expression of this enhancement, however, is seasonally dependent. For example, Shanghai shows a very strong daytime radial gradient in May, whereas in October the gradient remains evident but is weaker. New York also shows a clearer urban-core enhancement in October than in May. In contrast, cities such as Barcelona, Istanbul and Mumbai show more redistributed or even non-monotonic PBLH structure, indicating that coastal advection and local stratification can weaken or reorganize the simple inland-type urban-core enhancement.

https://doi.org/10.5194/egusphere-2026-4950
Preprint. Discussion started: 28 September 2026

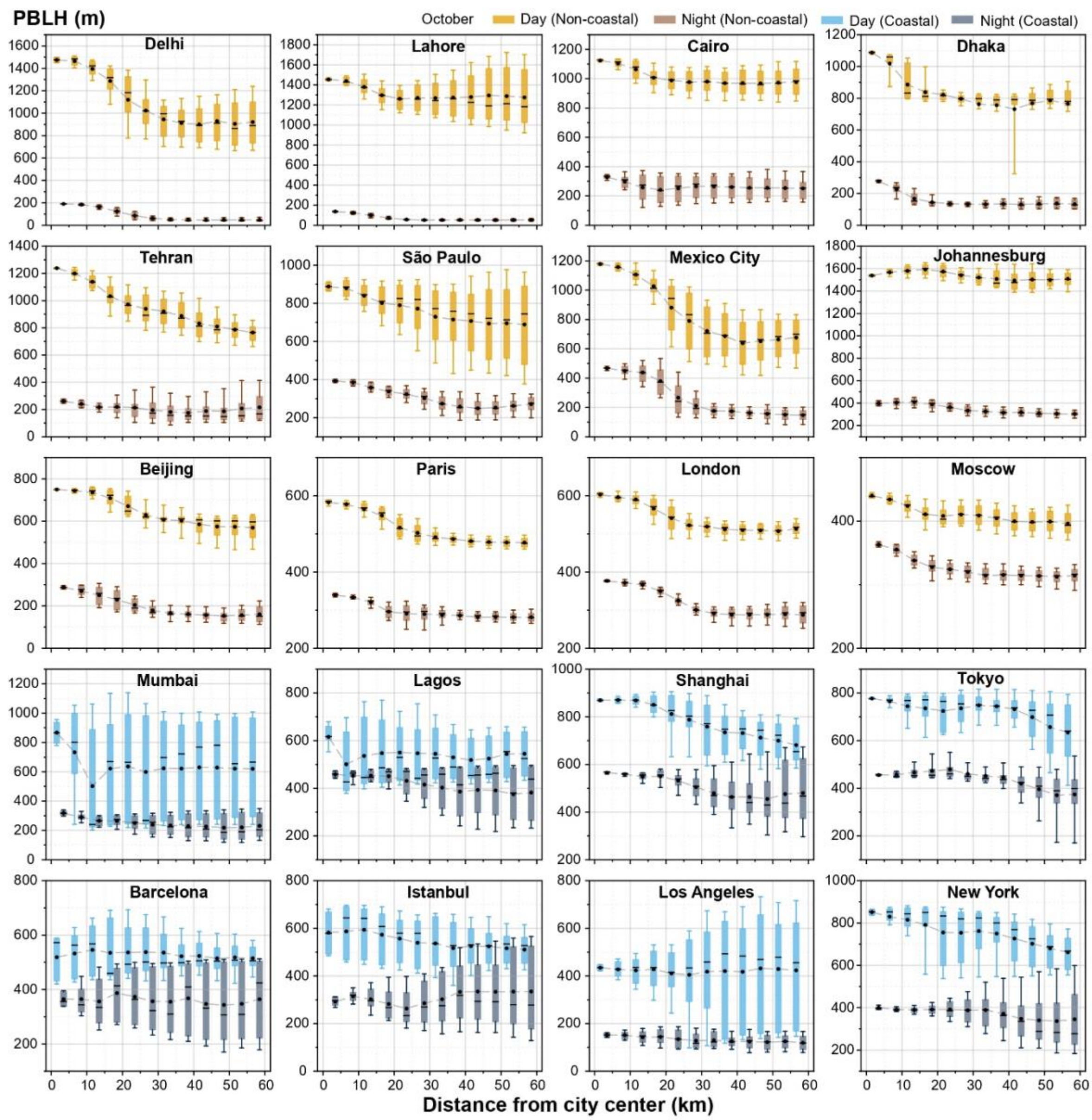

410 **Figure 3: Radial distributions of PBLH across the 20 megacities for October. Each city panel shows PBLH statistics in 5 km radial bands from the city centre to 60 km, with non-coastal cities arranged in the upper three rows and coastal cities in the lower two rows. Daytime and nighttime distributions are shown separately, with colours distinguishing day and night for the two city groups. Boxes represent the interquartile range (p25–p75), whiskers represent p10–p90, and black markers connected by dashed lines indicate the ring-wise mean.**

https://doi.org/10.5194/egusphere-2026-4950
Preprint. Discussion started: 28 September 2026

4.3 Radial change in wind speed

Figure 4 presents the ring-wise simulated WS distributions for October 2024 as a function of radial distance from the city centre (0–60 km) with corresponding May distributions in Supplement (Fig. S6). Across most cities (Fig. 4), WS is higher during the daytime than at night. Nighttime stability suppresses surface turbulence, thereby reducing near-surface wind speed. A common radial feature, particularly clear in non-coastal cities, is a near-surface wind-speed reduction in the inner rings (urban core), followed by an increase in WS with distance, particularly beyond approximately 15–30 km range. This classic urban wind-speed deficit is expected and is often more pronounced at night than during the day. Aerodynamic roughness and form drag within the urban core slow the near-surface flow (Wang et al., 2020). In inland cities with cropland-dominated surroundings, including Delhi, Lahore, Beijing, Paris, and London, the outward increase is relatively steep, consistent with a transition from dense roughness elements in the urban core to smoother rural terrain in the outer rings. Deviations from a simple, steadily increasing radial pattern occur mainly where terrain or basin structure modifies the background flow. Mexico City, Johannesburg, and São Paulo, for example, show irregular radial behaviour and broader distributions, consistent with the influence of complex terrain and basin-scale or slope-driven circulations (De Foy et al., 2006), as further illustrated by the corresponding spatial wind-speed fields (Figs. S26–S29).

Within the coastal ensemble, WS typically shows a smoother mean radial structure but larger within-ring spreads due to the variability in surface roughness in the radial rings (e.g sea is much smoother than urban and background surrounding land areas). Tokyo shows a comparatively muted radial contrast, consistent with earlier LULC results indicating that the outer rings remain substantially urbanized. Los Angeles shows a clearer urban wind reduction, while its broad distributions are consistent with a coastal-basin and terrain-gap setting, where slopes and gap flows may produce strong spatial variability, as evidenced by the corresponding spatial wind-speed fields (Figs. S26–S29). Shanghai also shows a distinct reduction in WS toward the urban core, consistent with earlier observational evidence of lower wind speeds in central Shanghai relative to nearby rural stations (Shun Djen, 1992)

When we compare the May and October WS, we find that the urban wind-speed deficit persists across seasons. However, the day-night contrast and the sharpness of the radial gradient are more evident in May than in October for some cities, particularly Delhi and Mexico City. The seasonal signal is especially clear in coastal cities, where May commonly shows broader within-ring spreads and a more redistributed radial structure, consistent with stronger land–sea thermal contrast and more active sea-breeze/land-breeze circulations.

https://doi.org/10.5194/egusphere-2026-4950
Preprint. Discussion started: 28 September 2026

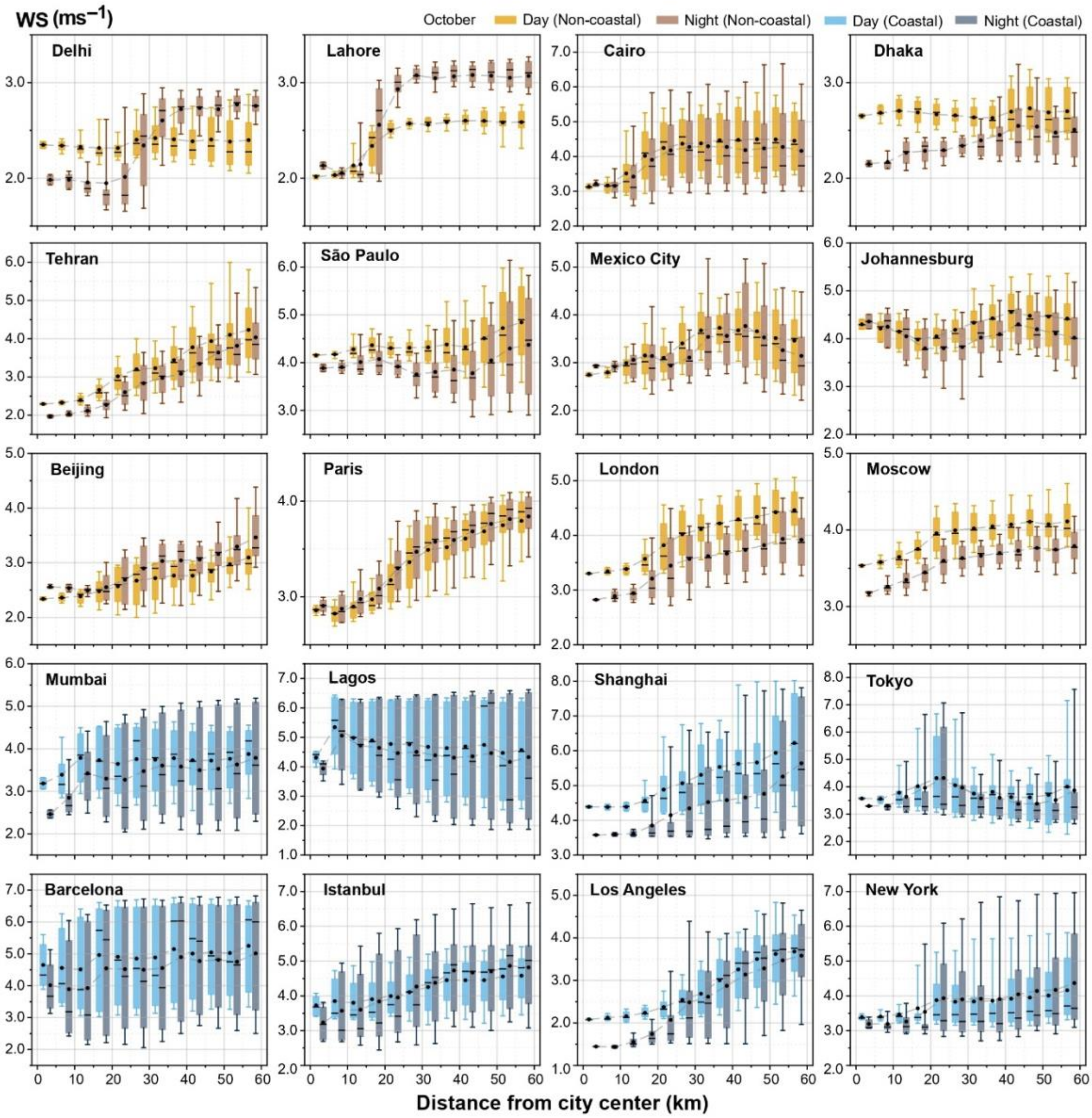

Figure 4: Radial distributions of WS across the 20 megacities for October. Each city panel shows WS statistics in 5 km radial bands from the city centre to 60 km, with non-coastal cities arranged in the upper three rows and coastal cities in the lower two rows. Daytime and nighttime distributions are shown separately, with colours distinguishing day and night for the two city groups. Boxes represent the interquartile range (p25–p75), whiskers represent p10–p90, and black markers connected by dashed lines indicate the ring-wise mean.

https://doi.org/10.5194/egusphere-2026-4950
Preprint. Discussion started: 28 September 2026

5 Urban–radial contrast

URC metric summarizes the radial ring analysis into a single, repeatable metric for each city and variable. While the ring-wise boxplots retain the full radial structure of the urban signal and the within-ring heterogeneity, URC provides a compact and repeatable measure for inter-city ranking and cross-variable comparison under a consistent sampling framework. It should be noted that, unlike URC-T, no elevation adjustment was applied to URC-PBLH and URC-WS as discussed in the methodology (Sect. 2.7). Consequently, the decomposition of URC-PBLH and URC-WS includes only the ocean-attributed component, which is applicable exclusively to coastal cities. For inland cities, the derived URC for PBLH and WS is therefore identical to the URC_{UA}. For each variable, the derived URC at all four analysis states is provided for all twenty cities in the Supplement (Figs. S9–S10) for URC-T, URC-PBLH, and URC-WS, respectively); the corresponding decomposition into ocean, elevation, and urbanization-attributed components is presented in the main text (Figs. 5 and 6).

5.1 URC of near-surface temperature

URC-T is directly analogous to the canopy-layer urban heat island intensity, with positive values indicating that the inner urban core is warmer than the surrounding reference environment. URC-T (Fig. S9) provides a concise quantitative measure of the urban rural thermal contrast across all twenty cities for both May and October 2024 under daytime and nighttime conditions and for each analysis state, denoted as $URC_{simulated}$, $URC_{ocean\text{-}adjusted}$, $URC_{elevation\text{-}adjusted}$, and $URC_{combined\text{-}adjusted}$, respectively. However, as discussed in Sect. 3, the simulated URC is inherently influenced by the characteristics of the reference environment. Consequently, the URC-T may either overestimate or underestimate the urbanization-induced component of the observed urban–rural thermal contrast. To quantify these environmental influences, the URC-T was decomposed into the ocean-attributed component (URC_{OA}-T), elevation-attributed component (URC_{EA}-T) and URC_{UA}-T (combined-adjusted), urbanization-attributed component (Fig. 5). It should be noted that the ocean-attributed component is zero for inland cities. Consequently, any difference between the simulated URC and URC_{UA} in inland cities arises solely from the elevation-attributed component.

Overall, URC-T remains predominantly positive across most cities even after both adjustments are applied, confirming that urban areas generally remain warmer than their surrounding environments. Furthermore, nocturnal URC_{UA}-T are consistently stronger than their daytime counterparts. Urban surfaces absorb and store a substantial fraction of incoming solar radiation during the day and, owing to their high heat capacity and thermal inertia, these surfaces gradually release this stored energy after sunset, thereby maintaining higher nighttime temperatures within the urban canopy. In addition, anthropogenic heat emissions from transportation, buildings, industrial activities, and air-conditioning systems further enhance nocturnal urban warming (Sun et al., 2026). During the daytime, however, the thermal contrast between the urban core and its surroundings is generally weaker because intense solar heating warms both urban and non-urban surfaces, while buoyancy-driven turbulence promotes a deeper convective boundary layer and stronger vertical mixing. Together, these processes reduce the near-surface

https://doi.org/10.5194/egusphere-2026-4950
Preprint. Discussion started: 28 September 2026

urban–rural temperature contrast, resulting in a substantially weaker daytime URC_{UA}-T and, sometimes, even reversing it. Accordingly, the following discussion focuses primarily on nighttime URC-T.

Among all the cities, the inland cities with low relief and extensive cropland surroundings, especially Delhi and Lahore (Sect. 3), show the strong urbanization-attributed component of the simulated urban–rural thermal contrast, with URC-T Changning negligibly after adjustment, indicating that the derived urban–rural thermal contrast is almost entirely attributable to urbanization. Delhi and Lahore record among the strongest nocturnal signals in the entire 20-city ensemble, with URC_{UA}-T of 5.0 °C (May) and 6.1 °C (October) for Delhi, and 4.0 °C (May) and 6.0 °C (October) for Lahore. Beijing, by contrast, shows a substantial URC_{EA}-T (~1.3 °C in both months), with nocturnal URC-T decreasing from 4.2 °C (May) and 4.0 °C (October) to URC_{UA}-T of 2.9 °C (May) and 2.7 °C (October), though its urbanization-attributed warming nonetheless remains among the strongest in the ensemble. Cairo shows a more moderate signal, with URC_{UA}-T of 2.6 °C in both months. The European cities also retain a clear nocturnal URC_{UA}-T, ranging from 1.4 to 3.7 °C, with only minor URC_{EA}-T contributions (0.2–0.4 °C in each city, reflecting modest elevation differences; Sect. 3). Paris shows a nocturnal URC-T of 3.6 °C (May) and 2.2 °C (October), decreasing only slightly to URC_{UA}-T of 3.3 °C (May) and 1.9 °C (October). Similarly, London exhibits URC_{UA}-T of 2.9 °C (May) and 1.5 °C (October). Moscow shows the strongest nocturnal URC_{UA}-T among the European cities in May (3.7 °C), decreasing to 1.4 °C in October.

Terrain-complex cities show substantially larger adjustments, with the elevation-attributed component (URC_{EA}-T) being positive (i.e. increasing the derived URC-T) in most cases, except for Johannesburg and São Paulo. A positive URC_{EA}-T indicates that the outer reference rings lie at a higher elevation than the urban core, so that part of their lower simulated temperatures reflects adiabatic cooling with altitude rather than the absence of urban forcing. Consequently, the derived URC-T is inflated, and accounting for elevation reduces the apparent urban–rural thermal contrast. This is clearest in Tehran, where nocturnal URC-T decreases from 7.3 °C (May) and 7.6 °C (October) to URC_{UA}-T of 3.3 °C (May) and 3.6 °C (October), with a URC_{EA}-T of almost exactly 4 °C in both months (teal bar, Fig. 5). The same behaviour occurs in Tehran's unusually large daytime URC-T. A similar pattern is observed in Mexico City, where nocturnal URC-T decreases from 5.1 °C (May) and 4.1 °C (October) to URC_{UA}-T of 3.2 °C (May) and 2.3 °C (October) after adjustment, with a URC_{EA}-T of just under 2 °C in both months, consistent with the pronounced basin topography described for Mexico City in Sect. 3. By contrast, São Paulo and Johannesburg show a negative URC_{EA}-T, indicating that their urban cores lie at slightly higher elevations than the surrounding reference environment. This explains the apparent daytime urban cool-island behaviour of Johannesburg i.e. its negative daytime URC-T (−0.4 °C in May; −0.9 °C in October) is primarily an elevation-induced effect, since the corresponding URC_{UA}-T values become positive in both months (0.7 °C in May; 0.3 °C in October), indicating a weak urbanization-induced daytime warming once elevation differences within the reference environment are accounted for. Similarly, São Paulo's nocturnal URC_{UA}-T strengthens from 2.4 °C (May) and 1.0 °C (October) to 3.0 °C (May) and 1.6 °C (October), with a URC_{EA}-T of −0.6 °C in both months, indicating that elevation suppresses rather than enhances the simulated URC-T, opposite to the behaviour observed in Tehran, Mexico City, and Beijing.

https://doi.org/10.5194/egusphere-2026-4950
Preprint. Discussion started: 28 September 2026

Overall, most cities in this inland group show a stronger urbanization attributed nocturnal warming signal in May than in October, except for Delhi, Lahore, and Dhaka, which show stronger nocturnal warming in October. Cairo, Tehran and Beijing show comparatively negligible seasonal differences. This divergence suggests that different regional meteorological regimes govern the seasonality of URC-T in different climate settings, rather than a single common driver. However, with only two representative months, we cannot draw firm conclusions about the annual seasonal cycle of URC-T from this comparison alone.

In coastal cities, the common behaviour is a nocturnal URC-T that remains markedly damped relative to that in inland cities, both before and after combined adjustment. The simulated nocturnal URC-T ranges from 0.7 to 2.1 °C across the group, with URC_{UA}-T widening to a range of −1.7 to 2.4 °C after accounting for both the ocean and elevation-attributed contributions. Part of this weaker contrast reflects sea-breeze/onshore-flow moderating the temperature of the urban core itself, most clearly evidenced along the coastal zones, especially in cities where the 60 km ring extends well inland, Barcelona and Los Angeles in particular, where the immediate coastal zone, including the urban core, is visibly cooler than the interior (Fig S14–S21).

A further contribution arises from the ocean-attributed component (URC_{OA}-T). As discussed in Sect. 4, ocean grid cells are typically warmer than adjacent land during the night because of the higher thermal inertia of the ocean surface. Consequently, their inclusion increases the mean temperature of the outer reference rings, thereby reducing the simulated URC-T and underestimating the urban–rural thermal contrast. Once ocean grid cells are excluded, the mean temperature of the outer rings decreases, resulting in higher URC_{UA}-T values. The opposite behaviour generally occurs during the daytime, when the ocean surface is typically cooler than the adjacent land. Barcelona, Istanbul, and Los Angeles additionally exhibit a substantial positive URC_{EA}-T, indicating that both ocean sampling and elevation differences contribute to the derived URC-T.

Among the coastal cities, Lagos, Shanghai, Istanbul, and Barcelona exhibit the strongest nocturnal urbanization-attributed warming, with URC_{UA}-T generally ranging from approximately 1.5 to 2.0 °C in both months. Mumbai and New York show their strongest URC_{UA}-T in October, reaching 2.4 °C in both cities. Mumbai also exhibits a pronounced daytime cooling signal in May, with URC_{UA}-T of −2.2 °C, comparable to that of Los Angeles. This behaviour reflects an asymmetric coastal–inland thermal contrast. The simulated spatial temperature field (Figs. S14–S17) shows that Mumbai's urban core, located adjacent to the coast, remains comparatively moderate, whereas the inland portion of Mumbai warms substantially more under intense May solar heating. This is consistent with Delhi and Lahore experiencing intense heating over the entire domain in May, and with the same onshore-flow moderation mechanism discussed above for Barcelona and Los Angeles. It should also be noted that, for Tokyo, URC_{UA}-T likely represents a conservative estimate of the true urbanization-attributed warming because the outer reference rings remain substantially urbanized (Sect. 3), a limitation independent of the methodological adjustments introduced here.

Los Angeles, the most terrain-complex of the coastal cities, shows the most unusual behaviour in the dataset: a simulated warming signal in both day and night that becomes a cooling signal in both periods after combined adjustments. This reflects its combined topographic and coastal setting. The 60 km reference ring includes the Angeles National Forest and San Gabriel range immediately north and northeast of the urban core, producing the largest and temporally consistent URC_{EA}-T of any

https://doi.org/10.5194/egusphere-2026-4950
Preprint. Discussion started: 28 September 2026

coastal city (approximately +3.7 °C during both daytime and nighttime in both months). The simulated spatial temperature fields (Figs. S14–S17) show that the region beyond these mountain ranges is the warmest part of the domain and becomes warmer after the elevation adjustment (Figs. S18–S21), indicating that the observed behaviour cannot be explained solely by elevation differences. Instead, it points to genuinely different climates. The corresponding WS fields (Figs. S26–S29) independently support this interpretation by showing the urban core within a pronounced wind-speed minimum, whereas the sector beyond the mountain range exhibits substantially stronger winds. Land-use mapping (Google Earth) further indicates that this sector is dominated by dry chaparral and shrubland. With limited moisture available for evaporation, incoming solar energy is converted predominantly into sensible heat flux rather than latent heat, consistent with the anomalously high temperatures. Together, these findings indicate that the urban core and the northern sector represent two distinct climatic regimes rather than a single, homogeneous reference environment.

Thus, it is worth noting that the framework is best suited to settings where the reference environment has a broadly uniform land-cover type, broadly radial urban growth and has a somewhat similar climatic regime, as is generally the case for most cities. It requires more careful interpretation in the cities, where the outer rings can span a mix of land, water, and, in the most extreme cases, complex terrain. In such settings, the URC_{UA}-T is better understood as the contrast between the urban core and this composite reference environment, rather than as a signal isolated from all non-urban influences

https://doi.org/10.5194/egusphere-2026-4950
Preprint. Discussion started: 28 September 2026

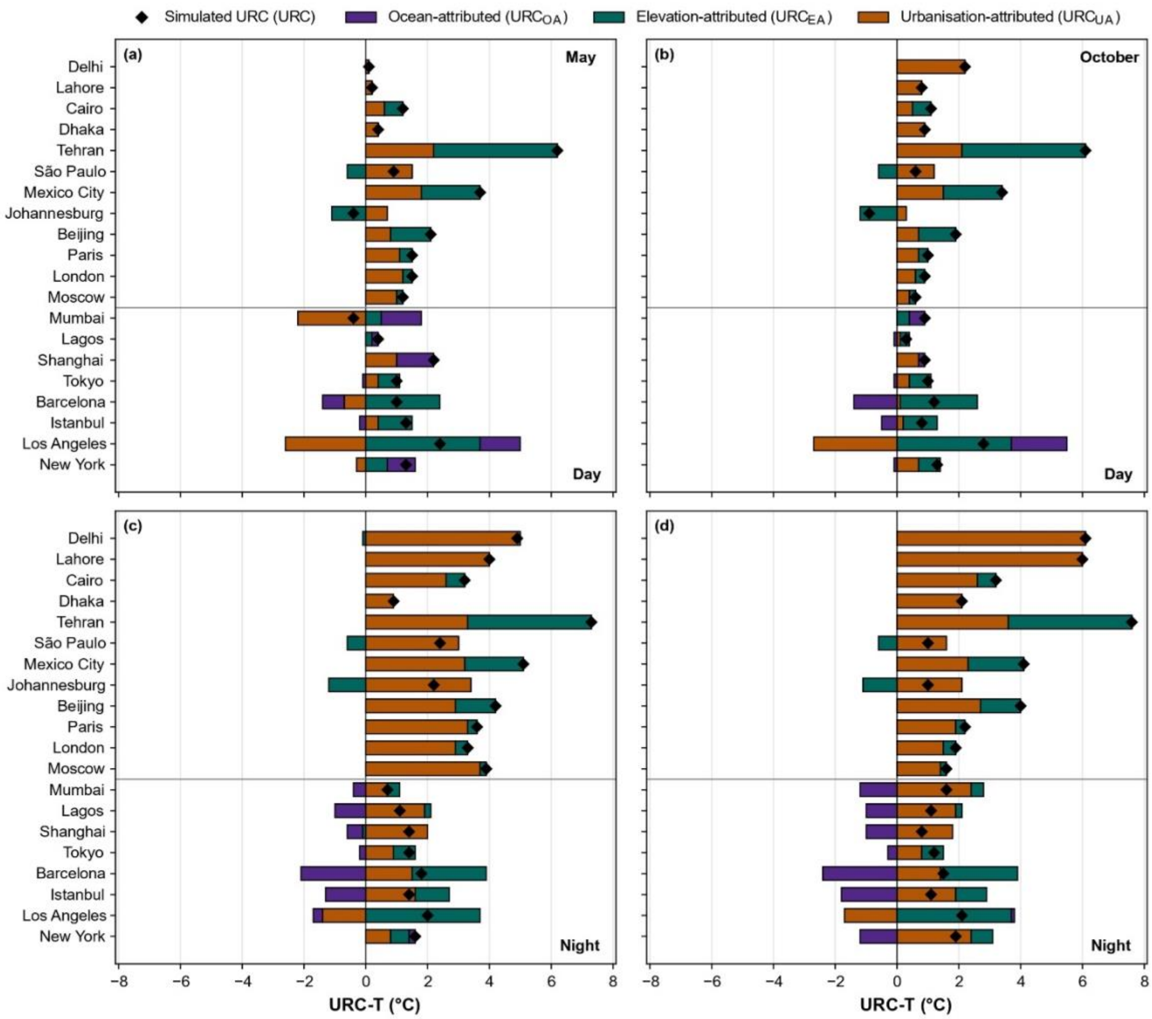

Figure 5: Decomposition of the derived Urban–radial Contrast (URC) in near-surface 2m temperature (URC-T) into its urbanization-attributed (URC_{UA}-T), elevation-attributed (URC_{EA}-T), and ocean-attributed (URC_{OA}-T) components, following Eqs. (4)–(7) (Sect. 2.7), for daytime (a, b) and nighttime (c, d) conditions in May (a, c) and October (b, d). For each city, coloured segments are stacked cumulatively from zero, in the order URC_{UA} (orange), URC_{EA} (teal), and, for coastal cities only, URC_{OA} (purple); the black diamond marks the resulting endpoint corresponding to the simulated URC-T (URC). URC_{OA} is defined only for the 8 coastal cities (lower group in each panel, separated from the 12 non-coastal cities by the horizontal line), since ocean adjustment was not applied to inland cities.

5.2 URC of PBLH

In most inland cities, URC-PBLH (identical to URC_{UA}-PBLH) is positive, especially during the daytime, indicating a deeper boundary layer and therefore enhanced vertical mixing over the urban core (Fig. 6). Daytime boundary-layer development is primarily controlled by the surface buoyancy flux, with mechanically generated turbulence (driven by wind shear and surface roughness) providing an additional contribution. Over the urban core, both effects act in the same direction: enhanced sensible

https://doi.org/10.5194/egusphere-2026-4950
Preprint. Discussion started: 28 September 2026

heat flux strengthens the convective boundary layer, while the increased aerodynamic roughness of the urban canopy further enhances mechanical mixing. This combination allows urban cores for inland cities to develop a substantially deeper daytime boundary layer height than their surroundings. At night, nocturnal boundary-layer depth is governed primarily by mechanically generated turbulence, which depends on surface roughness and wind shear rather than on solar heating. Because urban cores retain elevated roughness and act as a residual heat source through stored heat release, their nocturnal boundary layer remains less collapsed than that of the surrounding rural reference, so URC-PBLH for inland cities typically remains positive at night as well, despite absolute nighttime PBLH being far shallower than its daytime counterpart in both the urban core and its surroundings.

Among the inland cities, URC-PBLH is strongest for Tehran (592 and 405 m), Mexico City (489 and 483 m), and São Paulo (333 and 176 m) in May and October, respectively. All three were identified in Sect. 3 as terrain-complex cities, especially Tehran. In Tehran, a sharply peaked daytime PBLH maximum centred over the urban core decreases rapidly towards the much shallower boundary layer over the Alborz foothills to the north, well within the 60 km reference rings (Figs. S22–S25). The shallow PBLH over this mountainous sector, therefore, represents a genuine terrain-induced suppression of boundary-layer development rather than an artefact, contributing substantially to Tehran's exceptionally large URC-PBLH. Beijing (239 and 170 m), Paris (232 and 97 m), and London (233 and 87 m) likewise exhibit substantial daytime URC-PBLH, with all three decreasing markedly from May to October. Dhaka, in contrast, increases from 99 to 224 m, whereas Moscow shows the largest proportional seasonal decline, from 176 to 35 m, consistent with the overall reduction in daytime PBLH during October, as evident in the radial profiles. Delhi and Lahore show the clearest seasonal contrasts in the inland group. Delhi's daytime URC-PBLH strengthens substantially, from 35 m (May) to 526 m (October), whereas Lahore changes from −16 m (May) to 138 m (October), becoming the only inland city to change sign between the two months. This is consistent with reduced urban–rural contrast under the intense, spatially uniform heating and turbulent mixing of the pre-monsoon season, rather than a weaker urban effect specifically at these two cities.

The urban influence on PBLH in inland cities remains evident at night as well, though the absolute magnitudes are generally smaller than during the day. This reflects the overall shallow nocturnal boundary layer, consistent with the reduced role of buoyancy discussed above, leading to a lower-magnitude nighttime urban–rural contrast. Nocturnal URC-PBLH is largely governed by mechanically generated wind-shear turbulence, with the relatively warm urban core providing a secondary, weak buoyancy-related turbulence contribution on top of this. The strongest nighttime enhancement with occurs in Mexico City (183 and 301 m), Beijing (175 and 113 m), São Paulo (161 and 117 m), Moscow (133 and 39 m), Delhi (132 and 131 m), and Lahore (133 and 67 m) in May and October, respectively. Johannesburg (103 and 98 m) and Paris (96 and 50 m) exhibit more moderate nighttime URC-PBLH. Tehran (96 and 36 m) is notable because its nighttime enhancement remains relatively modest despite its exceptionally large daytime URC-PBLH, indicating a much stronger diurnal contrast than in most inland cities. The nighttime PBLH spatial field (Figs. S23 and S25) suggests that the boundary layer over the same mountainous sector retains some locally enhanced depth, mostly due to mechanically generated turbulence over complex terrain, thereby reducing the relative urban–rural contrast. Even these modest nighttime URC-PBLH values remain meteorologically important, since the

https://doi.org/10.5194/egusphere-2026-4950
Preprint. Discussion started: 28 September 2026

outer reference typically has a very shallow nocturnal boundary layer, so a positive nighttime URC indicates a substantial relative enhancement of urban mixing depth.

In coastal cities, URC-PBLH is considerably smaller than in most inland cities during the daytime, in both the simulated and ocean-adjusted analyses, with Shanghai (URC-PBLH: 362 m; URC_{UA}-PBLH: 176 m; May) the main exception. This weaker response is consistent with sea-breeze moderation of the urban core. Since daytime boundary-layer growth is primarily buoyancy-driven, thermal moderation of the coastal urban core reduces the sensible heat flux contrast between the urban core and the surrounding reference environment, thereby weakening URC-PBLH relative to inland cities. During the daytime, URC_{OA}-PBLH is generally positive because ocean grid cells develop a shallower boundary layer than adjacent land. Their inclusion, therefore, lowers the mean PBLH of the outer reference rings, apparently increasing the simulated URC-PBLH. Removing the ocean grid cells increases the outer-ring mean PBLH, thereby lowering URC_{UA}-PBLH.

Nighttime URC-PBLH in several coastal cities becomes comparable in magnitude to the inland cities, despite the much weaker daytime signal discussed above. Lagos (202 and 161 m) and Mumbai (155 and 140 m) exhibit the strongest nighttime URC_{UA}-PBLH in May and October, respectively. At night, URC_{OA}-PBLH becomes negative, opposite to the daytime behaviour. Because the ocean retains a comparatively deeper nocturnal boundary layer than adjacent land, its inclusion increases the mean PBLH of the outer reference rings, thereby reducing the simulated URC-PBLH. Consequently, removing the ocean grid cells increases URC_{UA}-PBLH, with the largest ocean-attributed contributions occurring in Barcelona, Mumbai, and Lagos.

5.3 URC of wind speed

URC-WS quantifies the difference in near-surface wind speed between the urban core and its outer reference environment. Since buildings and other urban structures greatly increase aerodynamic roughness compared with open land, water, or vegetated surfaces, increased drag on near-surface airflow reduces wind speed over the urban core relative to its surroundings. The simulated URC-WS (which is equivalent to URC_{UA}-WS for inland cities) and the URC_{UA}-WS for coastal cities (Fig. 6) are accordingly negative across most cities during both daytime and nighttime in May and October. Among the inland cities with simple, low-relief topography, the URC-WS is modest and fairly consistent between day and night. Lahore (-0.8 m s^{-1} in May (day), -1.0 m s^{-1} at night in both months) and Cairo range between -1.3 m s^{-1} in May (day) and -0.9 m s^{-1} in May (night), showing the clearest and most persistent URC-WS in this group. Among the European cities, London shows the largest URC-WS, strengthening from -0.5 m s^{-1} (May) to -1.1 m s^{-1} (October) during the day, with a comparable nighttime pattern (-0.4, -1.0 m s^{-1}); Paris and Moscow show smaller, broadly similar deficits in both periods.

In terrain-complex inland cities. Tehran exhibits the strongest URC-WS, ranging from -1.7 to -1.8 m s^{-1} during the daytime and remaining close to -1.8 m s^{-1} throughout the nighttime in both months. This behaviour is consistent with the exceptionally large URC-T and URC-PBLH reported for this city and reflects topographical influence on the pronounced contrast between the urban core and the surrounding mountainous terrain, evident in the spatial fields (Fig. S26–S29). Mexico City exhibits a substantial but smaller URC-WS, ranging from -0.9 to -0.7 m s^{-1} during the daytime and -1.2 to -0.3 m s^{-1} during the

https://doi.org/10.5194/egusphere-2026-4950
Preprint. Discussion started: 28 September 2026

nighttime. Johannesburg represents a clear exception, with URC-WS remaining close to zero or becoming slightly positive under some conditions (0.1 m s^{-1}; daytime, May and nighttime, October).

Coastal cities exhibit a weaker and more variable URC-WS than inland cities after accounting for the ocean-attributed contribution. The URC_{OA}-WS contribution provides a consistent and, in this respect, distinctive explanation: unlike URC-T and URC-PBLH, where the ocean's influence reverses direction between day and night due to its thermal inertia, the ocean's effect on URC-WS acts in the same direction at both times of day. Because the ocean surface is aerodynamically much smoother than land, wind speeds over open water are higher than over land regardless of solar heating. Including ocean grid cells in the outer ring, therefore, raises the reference wind speed in both day and night, making the simulated URC more strongly negative than the true land-based contrast. Removing ocean grid cells from the reference environment, therefore, reduces this contribution, increasing URC_{UA}-WS in nearly every coastal city and period.

Lagos is the only city in the ensemble with a clearly positive URC_{UA}-WS, especially at nighttime. It exhibits a simulated nighttime URC-WS of only 0.2–0.3 m s^{-1}, increasing to URC_{UA}-WS of 1.5 m s^{-1} (May) and 1.4 m s^{-1} (October) after accounting for the ocean-attributed contribution. With URC_{OA}-WS exceeding 1 m s^{-1} in both months, Lagos represents by far the largest ocean-attributed contribution identified in this study. Shanghai, Istanbul, and New York likewise exhibit substantial URC_{OA}-WS during the nighttime (approximately 0.6–1.3 m s^{-1}), although none approach the magnitude observed in Lagos, and none become positive after accounting for the ocean-attributed contribution. Los Angeles represents the clearest exception to the general coastal behaviour. URC_{OA}-WS remains comparatively small (approximately 0.2 m s^{-1}) during both daytime and nighttime, and the city retains the strongest coastal urban wind-speed deficit, with URC_{UA}-WS ranging from −1.3 to −1.4 m s^{-1} during the daytime and from −1.6 to −1.8 m s^{-1} during the nighttime, comparable to Tehran among the inland cities. This behaviour is consistent with the interpretation presented in Sect. 5.1 that Los Angeles' wind-speed deficit is governed primarily by its complex terrain and coastal setting rather than by ocean sampling. Tokyo exhibits a small but consistently positive URC_{UA}-WS, ranging from 0.1 to 0.4 m s^{-1} during both daytime and nighttime. This behaviour may be related to the substantially urbanized outer reference rings, already identified as a limitation for URC-T and URC-PBLH (Sects. 3 and 5.2).

https://doi.org/10.5194/egusphere-2026-4950
Preprint. Discussion started: 28 September 2026

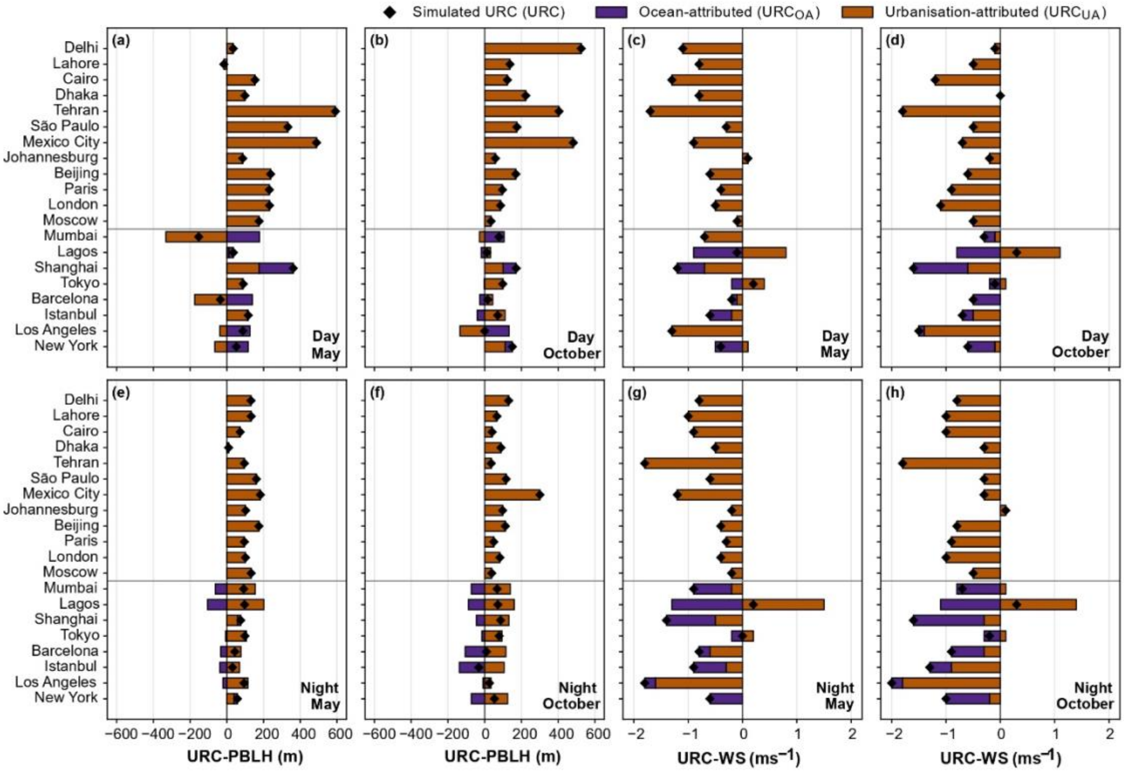

Figure 6: Decomposition of the derived Urban–Rural Contrast (URC) in planetary boundary layer height (URC-PBLH; a, b, e, f) and 10 m wind speed (URC-WS; c, d, g, h) into their urbanization-attributed (URC_{UA}-WS) and ocean-attributed (URC_{OA}-WS) components, for May (a, c, e, g) and October (b, d, f, h), under daytime (a-d) and nighttime (e-h) conditions, as labelled in each panel. As no elevation adjustment is applied to URC-PBLH or URC-WS (Sect. 2.7), each simulated value is decomposed into only these two components. URC_{OA} is defined only for the 8 coastal cities (lower group in each panel, separated from the 12 non-coastal cities by the horizontal line); for non-coastal cities, URC_{UA} is therefore identical to the diagnosed URC. For each city, coloured segments are stacked cumulatively from zero, in the order URC_{UA} (orange) and, for coastal cities only, URC_{OA} (purple), with the black diamond marking the resulting endpoint, corresponding to the simulated URC (URC-PBLH or URC-WS). Positive URC-PBLH indicates a deeper boundary layer over the urban core than over the reference environment; negative URC-WS indicates a wind-speed deficit at the urban core relative to the reference environment.

6 Overall URC response by non-coastal and coastal settings

To provide a broader comparison of how urbanization modifies key meteorological parameters across contrasting environments, we averaged the city-level URC values separately for non-coastal and coastal megacities, at each of the four analysis states defined in Sect. 2.7 and (Fig. S12 for URC-T, Fig. S11 for URC-PBLH and URC-WS). The grouped means URC (Fig. 7) confirm, and in one respect sharpen, the city-level contrasts already discussed in Sect. 5.

https://doi.org/10.5194/egusphere-2026-4950
Preprint. Discussion started: 28 September 2026

For URC-T, the non-coastal group remains clearly positive at every analysis state, in both day and night (Fig. 7). The elevation adjustment reduces the non-coastal mean by roughly a third in both periods (daytime: 1.55 to 0.97 °C in May and 1.55 to 0.99 °C in October; nighttime: 3.75 to 3.18 °C in May and 3.40 to 2.83 °C in October), indicating that inland urban cores remain consistently warmer than their surrounding reference environments, particularly during the nighttime when URC_{UA}-T remains close to 3 °C. The coastal group exhibits a markedly different evolution. During the nighttime, URC_{OA}-T increases the mean URC-T from 1.42 to 2.12 °C (May) and 1.41 to 2.51 °C (October), whereas URC_{EA}-T subsequently reduces these values to 0.78 and 0.75 °C, respectively (Fig. S12). The resulting URC_{UA}-T is 1.00 °C (May) and 1.36 °C (October) (Fig. 7), remaining positive but substantially weaker than the non-coastal group. During the daytime, the coastal mean decreases progressively across the decomposition and URC_{UA}-T becomes negative in both months (−0.50 °C in May; −0.06 °C in October) (Fig. 7), primarily because of Los Angeles and, to a lesser extent, Mumbai and Barcelona (Sect. 5.1). This is the clearest example in the dataset of a grouped mean changing sign after accounting for URC_{OA}-T and URC_{EA}-T, demonstrating that the apparent daytime coastal warming cannot be interpreted solely as an urbanization signal without considering the characteristics of the reference environment.

A similar, although less pronounced, contrast is observed for URC-PBLH. The non-coastal group remains substantially larger than the coastal group throughout, with mean URC-PBLH of 221 and 210 m during the daytime (May and October, respectively) and 116 and 97 m during the nighttime (Fig. 7). In the coastal group, URC_{OA}-PBLH reduces the daytime mean from 70 m (May) and 75 m (October) to −28 and 42 m, respectively, producing a slightly negative mean in May. During the nighttime, however, URC_{OA}-PBLH acts in the opposite direction, increasing the coastal mean from 74 to 103 m (May) and 45 to 114 m (October), bringing it close to, and in October slightly exceeding, the non-coastal nighttime mean. This behaviour mirrors the opposite daytime and nighttime response of URC_{OA}-PBLH identified at the city level (Sect. 5.2) and indicates that coastal urban cores develop a boundary layer approximately 100 m deeper than their surrounding land-based reference environment during the nighttime once the ocean-attributed contribution is accounted for.

URC-WS exhibits the most consistent behaviour of the three variables. The non-coastal group remains close to −0.7 m s^{-1} throughout the daytime and nighttime in both months, indicating little sensitivity to season or diurnal cycle. The coastal group initially exhibits a stronger simulated nighttime deficit (−0.78 to −0.93 m s^{-1}) than the non-coastal group (−0.69 to −0.72 m s^{-1}). However, URC_{OA}-WS substantially weakens this deficit during both daytime and nighttime, increasing URC_{UA}-WS to approximately −0.19 to −0.24 m s^{-1}. Consequently, the coastal group's urbanization-attributed wind-speed deficit becomes consistently weaker than that of the non-coastal group, opposite to the behaviour observed for URC-T and URC-PBLH.

Taken together, the grouped comparison confirms that non-coastal megacities exhibit a stronger and more consistent urbanization-attributed signal (URC_{UA}) than coastal megacities across all three meteorological variables. The coastal daytime thermal response is particularly sensitive to the characteristics of the reference environment, with URC_{UA}-T becoming negative on average after accounting for URC_{OA}-T and URC_{EA}-T, whereas the initially stronger coastal wind-speed deficit is substantially weakened once URC_{OA}-WS is removed. These grouped results reinforce the city-level analysis and demonstrate

https://doi.org/10.5194/egusphere-2026-4950
Preprint. Discussion started: 28 September 2026

that separating urbanization-attributed signals from ocean- and elevation-related contributions provides a more physically consistent basis for inter-city comparison.

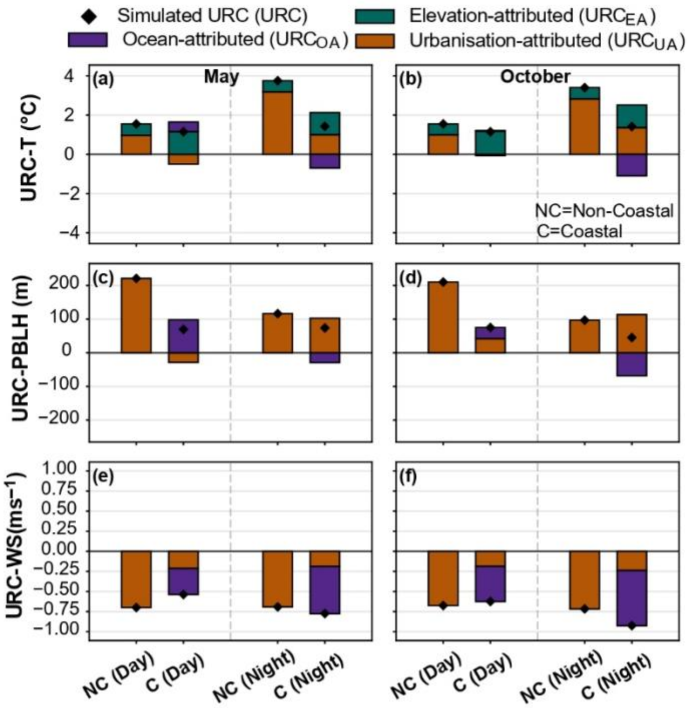

Figure 7: Grouped mean decomposition of the derived Urban–radial Contrast (URC) into its urbanization-attributed (URC$_{UA}$), elevation-attributed (URC$_{EA}$), and ocean-attributed (URC$_{OA}$) components, for near-surface temperature (URC-T; a, b), planetary boundary layer height (URC-PBLH; c, d), and 10 m wind speed (URC-WS; e, f), in May (a, c, e) and October (b, d, f). Group means were computed by first averaging each analysis state (simulated, ocean-adjusted, elevation-adjusted, and combined-adjusted) across the 12 non-coastal and 8 coastal cities separately, then applying Eqs. (4)–(7) (Sect. 2.7) to the resulting group-mean values. As no elevation adjustment is applied to URC-PBLH or URC-WS, URC$_{EA}$ is zero by definition for these variables. For each group, positive-valued components are stacked cumulatively above zero and negative-valued components are stacked cumulatively below zero, in the order URC$_{UA}$, URC$_{EA}$, URC$_{OA}$; the black diamond marks the group-mean simulated URC (the algebraic sum of all components). URC$_{OA}$ is zero for the non-coastal group by construction, since no ocean adjustment was required, and elevation adjustment applies only to URC-T.

7. Conclusions

This study develops and demonstrates a transferable and reproducible framework to quantify how urbanization modifies near-surface meteorology across megacities, with direct relevance to urban air quality. We focused on near-surface 2 m temperature (T), planetary boundary layer height (PBLH), and 10 m wind speed (WS), which together regulate urban warming, atmospheric mixing, and ventilation, and therefore pollutant dispersion.

https://doi.org/10.5194/egusphere-2026-4950
Preprint. Discussion started: 28 September 2026

The principal methodological contribution is a radial-analysis framework, combined with the Urban–radial contrast (URC) metric, that tracks how each variable evolves with distance from the city centre and decomposes the derived URC into an ocean component (URC_{OA}), an elevation component (URC_{EA}), and the urbanization-attributed component (URC_{UA}). This provides a consistent basis for inter-city, inter-season, and cross-variable comparison, while explicitly attributing the extent to which the diagnosed urban signal reflects the sampled reference environment rather than urbanization itself. Across the 20 megacities, the framework captured urban signatures in both May and October, including warmer urban cores, deeper urban mixing layers, and reduced near-surface wind speeds. The strongest URC_{UA}-T occurred at nighttime in Delhi (5.0 and 6.1 °C) and Lahore (4.0 and 6.0 °C) in May and October, respectively, whereas Tehran exhibited the largest elevation-attributed contribution (URC_{EA}-T ≈ 4 °C), reducing the simulated nighttime URC-T from 7.6 to 3.6 °C. Mexico City showed a similar but smaller reduction, while Johannesburg changed from an apparent daytime urban cool island (−0.9 °C) to weak warming (0.3 °C) after accounting for elevation. At the grouped level, non-coastal cities maintained substantially stronger nighttime URC_{UA}-T than coastal cities (3.18–2.83 °C versus 1.00–1.36 °C), whereas the coastal daytime URC_{UA}-T became negative after accounting for URC_{OA} and URC_{EA}.

Urban enhancement of boundary-layer depth was likewise substantially stronger in inland cities. Daytime URC-PBLH reached 592 and 405 m in Tehran, 489 and 483 m in Mexico City, and 35 and 526 m in Delhi during May and October, respectively. At the grouped level, mean daytime URC-PBLH for non-coastal cities was 221 and 210 m in May and October, respectively, compared with 70 and 75 m for the coastal group. After accounting for ocean attribution, the corresponding coastal means decreased to −28 and 42 m, respectively. Although smaller in absolute magnitude, nighttime URC-PBLH remained meteorologically important because of the shallow nocturnal boundary layer. Mean nighttime URC-PBLH for inland cities was 116 and 97 m, whereas coastal cities increased from 74 and 45 m to 103 and 114 m after accounting for URC_{OA}-PBLH, indicating that the ocean-attributed component enhances rather than suppresses the nighttime urban-rural contrast. In contrast to URC-T and URC-PBLH, URC-WS remained negative across both groups and seasons, indicating consistently weaker urban-core ventilation. The strongest nocturnal wind-speed deficits occurred in Tehran (−1.8 m s^{-1} in both months) and Los Angeles (URC_{UA}-WS: −1.6 to −1.8 m s^{-1}). Shanghai exhibited a comparably large simulated deficit (−1.4 to −1.6 m s^{-1}), which weakened substantially after accounting for URC_{OA}-WS, yielding URC_{UA}-WS of approximately −0.3 to −0.5 m s^{-1}. At the grouped level, inland cities maintained a remarkably consistent URC-WS of approximately −0.7 m s^{-1} throughout the daytime and nighttime in both months. Coastal cities initially exhibited a stronger simulated nighttime deficit (−0.78 to −0.93 m s^{-1}), but this weakened substantially after accounting for URC_{OA}-WS, increasing URC_{UA}-WS to approximately −0.19 to −0.24 m s^{-1}.

As urbanization continues to accelerate worldwide, particularly across rapidly growing megacities, these changes are expected to have substantial impacts on the urban environment and, ultimately, on long-term human well-being. The diagnostics developed here provide physically based inputs for reduced-complexity models that can efficiently estimate how future urban expansion may modify urban meteorology and its subsequent effects on pollutant dispersion, population exposure, and associated environmental risks, without requiring computationally expensive regional simulations for every urban-growth

https://doi.org/10.5194/egusphere-2026-4950
Preprint. Discussion started: 28 September 2026

scenario. By linking urbanization-driven meteorological change to air quality and exposure, the framework provides a foundation for evaluating future environmental risks and supporting evidence-based urban planning and climate adaptation.

Nevertheless, the framework has several limitations. Outer rings in some large or complex megaregions may still include suburban or satellite development, so the reference environment is not always purely rural even after adjustment. The elevation adjustment applies only to T, so URC-PBLH and URC-WS in topographically complex cities may retain an unresolved terrain-driven component. Furthermore, the framework is best suited for cities exhibiting somewhat radial urban growth patterns embedded within a broadly uniform reference environment and climate; applying this radial approach to highly asymmetric cities or highly heterogeneous surroundings requires careful interpretation. Additionally, the current framework does not employ an explicit urban canopy model and is therefore not intended to resolve street-scale processes. Finally, because the analysis draws on two representative months from a single year, it does not capture interannual variability.

Future work will couple the diagnosed meteorological changes with air-quality modelling to quantify how urbanization-driven changes in meteorology influence air pollution across megacities. Furthermore, the quantitative diagnostics developed in this study will provide the foundation for reduced-complexity modelling approaches that can efficiently evaluate future urban-growth scenarios and their implications for environmental quality, population exposure, and sustainable urban planning in rapidly expanding megacities.

Author contributions

AAW, SGu, and SGa conceptualized the study. AAW performed the formal analysis, prepared the visualizations, and wrote the original draft of the manuscript. SGu and SGa supervised the research. All authors contributed to the development of the methodology and to the review and editing of the manuscript. ChatGPT (OpenAI) was used to assist with grammar, sentence structure, and language clarity during manuscript preparation. All scientific content, analysis, and interpretation were developed by the authors.

Competing interests

The authors declare that they have no conflict of interest.

Acknowledgements

We dedicate this article to the memory of our co-author, Victoria Sinclair. Her contributions to this work were invaluable, and it was a privilege to work alongside her. She will be greatly missed.

https://doi.org/10.5194/egusphere-2026-4950
Preprint. Discussion started: 28 September 2026

Financial support

This work was supported by the European Commission through the Horizon Europe project FOCI (Grant agreement No. 101056783) and by the Research Council of Finland through the Atmosphere and Climate Competence Centre (ACCC) Flagship (Grant Nos. 337549, 3570902, and 359340) and the CO-ENHANCIN project (Grant No. 360114).

References

Arnfield, A. J.: Two decades of urban climate research: a review of turbulence, exchanges of energy and water, and the urban heat island, Intl Journal of Climatology, 23, 1–26, https://doi.org/10.1002/joc.859, 2003.

Babatola, S. S.: Global burden of diseases attributable to air pollution, J Public Health Afr, 9, 813, https://doi.org/10.4081/jphia.2018.813, 2018.

Baklanov, A., Molina, L. T., and Gauss, M.: Megacities, air quality and climate, Atmospheric Environment, 126, 235–249, https://doi.org/10.1016/j.atmosenv.2015.11.059, 2016.

Barlow, J. F.: Progress in observing and modelling the urban boundary layer, Urban Climate, 10, 216–240, https://doi.org/10.1016/j.uclim.2014.03.011, 2014.

Bauer, T. J.: Interaction of Urban Heat Island Effects and Land-Sea Breezes during a New York City Heat Event, Journal of Applied Meteorology and Climatology, 59, 477–495, https://doi.org/10.1175/JAMC-D-19-0061.1, 2020.

Budhiraja, B., Gawuc, L., and Agrawal, G.: Seasonality of Surface Urban Heat Island in Delhi City Region Measured by Local Climate Zones and Conventional Indicators, IEEE J. Sel. Top. Appl. Earth Observations Remote Sensing, 12, 5223–5232, https://doi.org/10.1109/JSTARS.2019.2955133, 2019.

Budhiraja, B., Agrawal, G., and Pathak, P.: Urban heat island effect of a polynuclear megacity Delhi – Compactness and thermal evaluation of four sub-cities, Urban Climate, 32, 100634, https://doi.org/10.1016/j.uclim.2020.100634, 2020.

Connors, J. P., Galletti, C. S., and Chow, W. T. L.: Landscape configuration and urban heat island effects: assessing the relationship between landscape characteristics and land surface temperature in Phoenix, Arizona, Landscape Ecol, 28, 271–283, https://doi.org/10.1007/s10980-012-9833-1, 2013.

Cui, Y. Y. and De Foy, B.: Seasonal Variations of the Urban Heat Island at the Surface and the Near-Surface and Reductions due to Urban Vegetation in Mexico City, Journal of Applied Meteorology and Climatology, 51, 855–868, https://doi.org/10.1175/JAMC-D-11-0104.1, 2012.

De Foy, B., Clappier, A., Molina, L. T., and Molina, M. J.: Distinct wind convergence patterns in the Mexico City basin due to the interaction of the gap winds with the synoptic flow, Atmos. Chem. Phys., 6, 1249–1265, https://doi.org/10.5194/acp-6-1249-2006, 2006.

Debbage, N. and Shepherd, J. M.: The urban heat island effect and city contiguity, Computers, Environment and Urban Systems, 54, 181–194, https://doi.org/10.1016/j.compenvurbsys.2015.08.002, 2015.

https://doi.org/10.5194/egusphere-2026-4950
Preprint. Discussion started: 28 September 2026

Guan, H., Kumar, V., Clay, R., Kent, C., Bennett, J., Ewenz, C., Hopkins, G., and Simmons, C. T.: Temporal and spatial patterns of air temperature in a coastal city with a slope base setting, JGR Atmospheres, 121, 5336–5355, https://doi.org/10.1002/2016JD025139, 2016a.

Guan, H., Kumar, V., Clay, R., Kent, C., Bennett, J., Ewenz, C., Hopkins, G., and Simmons, C. T.: Temporal and spatial patterns of air temperature in a coastal city with a slope base setting, Journal of Geophysical Research: Atmospheres, 121, 5336–5355, https://doi.org/10.1002/2016JD025139, 2016b.

Hu, Y., Tan, J., Grimmond, S., Ao, X., Yan, Y., and Liu, D.: Observed and Modeled Urban Heat Island and Sea-Breeze Circulation Interactions: A Shanghai Case Study, https://doi.org/10.1175/JAMC-D-20-0246.1, 2022.

Hurduc, A., Ermida, S. L., Trigo, I. F., and DaCamara, C. C.: Importance of temporal dimension and rural land cover when computing surface urban Heat Island intensity, Urban Climate, 56, 102013, https://doi.org/10.1016/j.uclim.2024.102013, 2024.

Jahangir, M. S. and Moghim, S.: Assessment of the urban heat island in the city of Tehran using reliability methods, Atmospheric Research, 225, 144–156, https://doi.org/10.1016/j.atmosres.2019.03.038, 2019.

Jauregui, E.: Heat island development in Mexico City, Atmospheric Environment, 31, 3821–3831, https://doi.org/10.1016/S1352-2310(97)00136-2, 1997.

Kumar, R., Mishra, V., Buzan, J., Kumar, R., Shindell, D., and Huber, M.: Dominant control of agriculture and irrigation on urban heat island in India, Sci Rep, 7, 14054, https://doi.org/10.1038/s41598-017-14213-2, 2017.

Li, D. and Bou-Zeid, E.: Synergistic Interactions between Urban Heat Islands and Heat Waves: The Impact in Cities Is Larger than the Sum of Its Parts, Journal of Applied Meteorology and Climatology, 52, 2051–2064, https://doi.org/10.1175/JAMC-D-13-02.1, 2013.

Li, Y., Zhang, J., Sailor, D. J., and Ban-Weiss, G. A.: Effects of urbanization on regional meteorology and air quality in Southern California, Atmospheric Chemistry and Physics, 19, 4439–4457, https://doi.org/10.5194/acp-19-4439-2019, 2019.

Li, Z., Guo, J., Ding, A., Liao, H., Liu, J., Sun, Y., Wang, T., Xue, H., Zhang, H., and Zhu, B.: Aerosol and boundary-layer interactions and impact on air quality, Natl Sci Rev, 4, 810–833, https://doi.org/10.1093/nsr/nwx117, 2017.

Liu, S. and Liang, X.-Z.: Observed Diurnal Cycle Climatology of Planetary Boundary Layer Height, https://doi.org/10.1175/2010JCLI3552.1, 2010.

Liu, Y., Qian, Y., Kaul, C. M., Gaudet, B. J., Berg, L. K., Feng, Z., Varble, A. C., Tai, S., Feng, Y., Yang, Z., Chakraborty, T. C., and Fast, J. D.: Urban Land Surface Effects on Summertime Clouds and Moist Convection in Houston Under Different Synoptic Conditions, JGR Atmospheres, 131, e2025JD045131, https://doi.org/10.1029/2025JD045131, 2026.

Lo, J. C. F., Lau, A. K. H., Chen, F., Fung, J. C. H., and Leung, K. K. M.: Urban Modification in a Mesoscale Model and the Effects on the Local Circulation in the Pearl River Delta Region, https://doi.org/10.1175/JAM2477.1, 2007.

Marlier, M. E., Jina, A. S., Kinney, P. L., and DeFries, R. S.: Extreme Air Pollution in Global Megacities, Curr Clim Change Rep, 2, 15–27, https://doi.org/10.1007/s40641-016-0032-z, 2016.

Martin-Vide, J., Sarricolea, P., and Moreno-García, M. C.: On the definition of urban heat island intensity: the “rural” reference, Front. Earth Sci., 3, https://doi.org/10.3389/feart.2015.00024, 2015.

https://doi.org/10.5194/egusphere-2026-4950
Preprint. Discussion started: 28 September 2026

Melecio-Vázquez, D., Ramamurthy, P., Arend, M., and González-Cruz, J. E.: Thermal Structure of a Coastal–Urban Boundary Layer, Boundary-Layer Meteorol, 169, 151–161, https://doi.org/10.1007/s10546-018-0361-7, 2018.

Park, K., Baik, J.-J., Jin, H.-G., and Tabassum, A.: Changes in urban heat island intensity with background temperature and humidity and their associations with near-surface thermodynamic processes, Urban Climate, 58, 102191, https://doi.org/10.1016/j.uclim.2024.102191, 2024.

Peng, W., Yang, X., and Chen, S. S.: Effect of the reference rural landscape on annual variations in surface urban heat island intensity, Sustainable Cities and Society, 115, 105804, https://doi.org/10.1016/j.scs.2024.105804, 2024.

Petäjä, T., Järvi, L., Kerminen, V.-M., Ding, A. J., Sun, J. N., Nie, W., Kujansuu, J., Virkkula, A., Yang, X., Fu, C. B., Zilitinkevich, S., and Kulmala, M.: Enhanced air pollution via aerosol-boundary layer feedback in China, Sci Rep, 6, 18998, https://doi.org/10.1038/srep18998, 2016.

Qiao, Z., Wang, N., Chen, J., He, T., Xu, X., Liu, L., Sun, Z., and Han, D.: Urbanization accelerates urban warming by changing wind speed: Evidence from China based on 2421 meteorological stations from 1978 to 2017, Environmental Impact Assessment Review, 102, 107189, https://doi.org/10.1016/j.eiar.2023.107189, 2023.

Rajeswari, J. R., Srinivas, C. V., Yesubabu, V., Hari Prasad, D., and Venkatraman, B.: Impacts of Urbanization, Aerodynamic Roughness, and Land Surface Processes on the Extreme Heavy Rainfall Over Chennai, India, Journal of Geophysical Research: Atmospheres, 126, e2020JD034017, https://doi.org/10.1029/2020JD034017, 2021.

Shun Djen, C.: The urban climate of Shanghai, Atmospheric Environment. Part B. Urban Atmosphere, 26, 9–15, https://doi.org/10.1016/0957-1272(92)90033-O, 1992.

Stewart, I. D. and Oke, T. R.: Local Climate Zones for Urban Temperature Studies, Bulletin of the American Meteorological Society, 93, 1879–1900, https://doi.org/10.1175/BAMS-D-11-00019.1, 2012.

Sun, Y., Oleson, K. W., and Zheng, Z.: Modeling Urban Traffic Heat Flux in the Community Earth System Model: Formulation and Validation for Two Test Sites, Journal of Advances in Modeling Earth Systems, 18, e2025MS005435, https://doi.org/10.1029/2025MS005435, 2026.

Tang, J., Lan, X., Lian, Y., Zhao, F., and Li, T.: Estimation of Urban–Rural Land Surface Temperature Difference at Different Elevations in the Qinling–Daba Mountains Using MODIS and the Random Forest Model, Int J Environ Res Public Health, 19, 11442, https://doi.org/10.3390/ijerph191811442, 2022.

United Nations (Ed.): World urbanization prospects 2025: summary of results, United Nations, New York, 1 pp., 2025.

Wang, J., Feng, J., Yan, Z., and Zha, J.: Urbanization Impact on Regional Wind Stilling: A Modeling Study in the Beijing-Tianjin-Hebei Region of China, Journal of Geophysical Research: Atmospheres, 125, e2020JD033132, https://doi.org/10.1029/2020JD033132, 2020.

Wang, M., Zhang, X., and Yan, X.: Modeling the climatic effects of urbanization in the Beijing–Tianjin–Hebei metropolitan area, Theor Appl Climatol, 113, 377–385, https://doi.org/10.1007/s00704-012-0790-z, 2013.

Wang, M., Tang, G., Liu, Y., Ma, M., Yu, M., Hu, B., Zhang, Y., Wang, Y., and Wang, Y.: The difference in the boundary layer height between urban and suburban areas in Beijing and its implications for air pollution, Atmospheric Environment, 260, 118552, https://doi.org/10.1016/j.atmosenv.2021.118552, 2021.

https://doi.org/10.5194/egusphere-2026-4950
Preprint. Discussion started: 28 September 2026

Wang, Y., Di Sabatino, S., Martilli, A., Li, Y., Wong, M. S., Gutiérrez, E., and Chan, P. W.: Impact of land surface heterogeneity on urban heat island circulation and sea-land breeze circulation in Hong Kong, JGR Atmospheres, 122, 4332–4352, https://doi.org/10.1002/2017JD026702, 2017.

Wu, Y., Li, S., and Yu, S.: Monitoring urban expansion and its effects on land use and land cover changes in Guangzhou city, China, Environ Monit Assess, 188, 54, https://doi.org/10.1007/s10661-015-5069-2, 2015.

Xiao, Y., Yang, J., Cui, L., Deng, J., Fu, P., and Zhu, J.: Weakened Sea-Land Breeze in a Coastal Megacity Driven by Urbanization and Ocean Warming, Earth's Future, 11, e2022EF003341, https://doi.org/10.1029/2022EF003341, 2023.

Yu, M., Liu, Y., Dai, Y., and Yang, A.: Impact of urbanization on boundary layer structure in Beijing, Climatic Change, 120, 123–136, https://doi.org/10.1007/s10584-013-0788-2, 2013.

Zargari, M., Mofidi, A., Entezari, A., and Baaghideh, M.: Climatology of Tehran surface heat Island: a satellite-based spatial analysis, Sci Rep, 15, 10567, https://doi.org/10.1038/s41598-025-95367-2, 2025.

Zhang, G., Azorin-Molina, C., Wang, X., Chen, D., McVicar, T. R., Guijarro, J. A., Chappell, A., Deng, K., Minola, L., Kong, F., Wang, S., and Shi, P.: Rapid urbanization induced daily maximum wind speed decline in metropolitan areas: A case study in the Yangtze River Delta (China), Urban Climate, 43, 101147, https://doi.org/10.1016/j.uclim.2022.101147, 2022a.

Zhang, Z., Paschalis, A., Mijic, A., Meili, N., Manoli, G., van Reeuwijk, M., and Fatichi, S.: A mechanistic assessment of urban heat island intensities and drivers across climates, Urban Climate, 44, 101215, https://doi.org/10.1016/j.uclim.2022.101215, 2022b.